


# Metabolic priming in G6PDH isoenzyme-replaced tobacco lines improves stress tolerance and seed yields via altering assimilate partitioning

Judith Scharte<sup>1</sup>, Sebastian Hassa<sup>1</sup>, Cornelia Herrfurth<sup>2</sup>, Ivo Feussner<sup>2</sup>, Giuseppe Forlani<sup>3</sup>, Engelbert Weis<sup>1</sup> and Antje von Schaewen<sup>1,\*</sup> 

<sup>1</sup>Institut für Biologie und Biotechnologie der Pflanzen, Fachbereich Biologie, Universität Münster, Schlossplatz 7, D-48149 Münster, Germany,

<sup>2</sup>Albrecht-von-Haller-Institut für Pflanzenwissenschaften and Göttinger Zentrum für Molekulare Biowissenschaften (GZMB), Abteilung Biochemie der Pflanze, Universität Göttingen, Justus-von-Liebig-Weg 11, D-37077 Göttingen, Germany, and

<sup>3</sup>Laboratorio di Fisiologia e Biochimica Vegetale, Dipartimento di Scienze della Vita e Biotechnologie, Università degli Studi di Ferrara, Via L. Borsari 46, I-44121 Ferrara, Italy

Received 9 January 2023; revised 25 August 2023; accepted 29 August 2023; published online 15 September 2023.

\*For correspondence (e-mail [schaewen@uni-muenster.de](mailto:schaewen@uni-muenster.de)).

## SUMMARY

We investigated the basis for better performance of transgenic *Nicotiana tabacum* plants with G6PDH-isoenzyme replacement in the cytosol (Xanthi::cP2::cytRNAi, Scharte et al., 2009). After six generations of selfing, infiltration of *Phytophthora nicotianae* zoospores into source leaves confirmed that defence responses (ROS, callose) are accelerated, showing as fast cell death of the infected tissue. Yet, stress-related hormone profiles resembled susceptible Xanthi and not resistant cultivar SNN, hinting at mainly metabolic adjustments in the transgenic lines. Leaves of non-stressed plants contained twofold elevated fructose-2,6-bisphosphate (F2,6P<sub>2</sub>) levels, leading to partial sugar retention (soluble sugars, starch) and elevated hexose-to-sucrose ratios, but also more lipids. Above-ground biomass lay in between susceptible Xanthi and resistant SNN, with photo-assimilates preferentially allocated to inflorescences. Seeds were heavier with higher lipid-to-carbohydrate ratios, resulting in increased harvest yields - also under water limitation. Abiotic stress tolerance (salt, drought) was improved during germination, and in floated leaf disks of non-stressed plants. In leaves of salt-watered plants, proline accumulated to higher levels during illumination, concomitant with efficient NADP(H) use and recycling. Non-stressed plants showed enhanced PSII-induction kinetics (upon dark–light transition) with little differences at the stationary phase. Leaf exudates contained 10% less sucrose, similar amino acids, but more fatty acids – especially in the light. Export of specific fatty acids via the phloem may contribute to both, earlier flowering and higher seed yields of the Xanthi-cP2 lines. Apparently, metabolic priming by F2,6P<sub>2</sub>—combined with sustained NADP(H) turnover—bypasses the genetically fixed growth–defence trade-off, rendering tobacco plants more stress-resilient and productive.

**Keywords:** G6PDH, isoenzyme replacement, *Nicotiana tabacum*, NADPH, stress tolerance, flowering, metabolic priming, assimilate partitioning, lipid synthesis, phloem exudates, seed yields.

## INTRODUCTION

When exposed to biotic stress (bacteria, fungi and viruses) or abiotic stress (drought, salt and extreme temperatures), plants divert most of their energy and resources towards defence responses and acclimation processes. Among the first detectable reactions of eukaryotic cells to stress conditions are bursts of reactive oxygen species (ROS) at the plasma membrane that rely on NADPH provision in the cytosol (reviewed in Mittler, 2017; Yu et al., 2017). In resistant plant varieties, pathogen recognition and

subsequent defence signalling lead to fast callose deposition at plasmodesmata, resulting in sugar retention within the infected source leaf tissue (Scharte et al., 2005, 2009). As a consequence, primary metabolism—and linked secondary metabolism—is stimulated in the closed-off areas to promote the biosynthesis of stress-specific compounds, which limits photosynthetic efficiency and long-distance assimilate transport. This phenomenon, known as growth–defence trade-off under stress (see the editorial by Eckardt, 2017), usually compromises the harvest yield of both

vegetative and reproductive plant tissues (reviewed in Allahverdiyeva et al., 2015; He et al., 2022; Leisner et al., 2022).

Attempts to improve stress resilience and biomass production of plant species that are relevant to humankind have a long tradition. Besides recent sophisticated breeding programs in staple crops (e.g. rice; Takatsuji, 2017), also transgenic approaches have been pursued. The latter mainly focused on aspects of *source* versus *sink* strength under stress (Murchie et al., 2023; Yu et al., 2015), photosynthetic parameters (Furbank et al., 2015; Nowicka et al., 2018), or photorespiratory losses (Engqvist & Maurino, 2017; Jin et al., 2022; South et al., 2019). Others set out to modulate cell-wall fortification (Wang et al., 2016), flowering time (Ionescu et al., 2017), stress signalling (Joshi et al., 2018; Tarkowski et al., 2022), or devised climate-smart combinations thereof (Jansson et al., 2018). In part, these approaches took advantage of mutants and gene stacking (Kudo et al., 2019), and/or the combination of crop lines that are resilient to multiple stresses (Rivero et al., 2022).

So far, engineering plant cultivars for improved stress tolerance has been attempted by disruption and/or overexpression of genes coding for suspected key players, and studying the effects in transgenic lines compared with the wild type under standardized growth conditions (Maggio et al., 2018). We also used this approach in the past to replace glucose-6-phosphate dehydrogenase (G6PDH) in the cytosol by an isoform with different kinetics in a susceptible *N. tabacum* variety (Scharte et al., 2009). G6PDH catalyses the rate-limiting step of the oxidative pentose-phosphate pathway (OPPP) that is an important route for sugar-based NADPH provision in both the cytosol and plastid stroma (reviewed in Kruger & von Schaewen, 2003). NADPH is the preferred electron donor in most anabolic pathways and also needed for oxidative bursts at the plasma membrane, later promoting recovery of redox homeostasis via the universal glutathione buffer (GSH/GSSG), due to strict NADPH-dependence of glutathione reductase (EC:1.8.1.7).

Mature *source* leaves of plants are specialized in assimilate export and sugar-driven transport to *sink* tissues by mass flow in the phloem (reviewed in Zhang & Turgeon, 2018). With the onset of pathogen infection, they close their plasmodesmata by synthesizing callose plugs wherefore assimilate export ceases and sugars backup. This measure activates primary metabolism, including the cytosolic G6PDH isoforms—not only by elevated substrate (G6P) availability, but also via *sugar sensing*-induced transcriptional upregulation (as shown for potato, Hauschild & von Schaewen, 2003). In Arabidopsis, stress signalling activates cytosolic isoform G6PD6 (At5g40760) by protein kinases ASK $\alpha$  and/or MPK3/MPK6 (Bhagat et al., 2022; Dal Santo et al., 2012; Stampfl et al., 2016). Resulting enhanced

flux through the irreversible OPPP reactions provides ample NADPH in the cytosol to support oxidative bursts by NADPH oxidase (plant respiratory burst oxidase homolog, Rboh) at the plasma membrane. This was shown for tobacco, first using elicited suspension culture cells of the *N. tabacum* cultivar Xanthi (Pugin et al., 1997) and then zoospore-challenged leaves of the hypersensitive *N. tabacum* cultivar Samsun NN (SNN), before comparing the responses of both varieties (Scharte et al., 2005, 2009).

Activated Rboh enzymes extrude superoxide ( $O_2^-$ ) into the acidic apoplast, where the unstable ROS is converted to metastable hydrogen peroxide ( $H_2O_2$ ) and enters the cytosol via aquaporins to initiate stress signalling (for review see Mittler, 2017).  $H_2O_2$  dissipation in the cytosol involves peroxiredoxins (Prx) and other members of the thioredoxin (Trx) superfamily, promoting redox switches in cognate target enzymes, thus altering their activity and/or subcellular localization (Baune et al., 2020; Meyer et al., 2011; Wakao & Benning, 2005). Intersection with kinase cascades leads to phosphorylation of target proteins (e.g. Arabidopsis G6PD6 at a conserved Thr residue, Dal Santo et al., 2012; Stampfl et al., 2016), and further adjustments to the changed condition (Dietz et al., 2016; Leisner et al., 2022, and references cited therein). Thus, increased flux through the irreversible OPPP reactions does not only support oxidative bursts at the plasma membrane, followed by redox signalling and recovery, but may also promote the biosynthesis of specific compounds needed for stress adaptation and/or development: for example, proline with protective roles under both abiotic (Giberti et al., 2014; Sabbioni et al., 2021) and biotic stress conditions (Okumoto et al., 2016; reviewed in Alvarez et al., 2022). Of note, ROS signalling also shapes plant architecture in response to nutritional cues (Tarkowski et al., 2022).

Based on the characteristics of cytosolic and plastidic G6PDH isoenzymes from potato (von Schaewen et al., 1995; Wenderoth et al., 1997; Wendt et al., 2000), we engineered the susceptible *N. tabacum* cultivar Xanthi for improved NADPH provision in the cytosol using an isoenzyme of heterotrophic plastids with less NADPH-feedback inhibition (P2 class; Wendt et al., 2000). Arabidopsis *G6PD3* was amplified without transit peptide, placed under the control of a strong constitutive promoter (CaMV 35S; from cauliflower mosaic virus) and introduced into the tobacco Xanthi variety via Agrobacterium-mediated leaf transformation. Among the regenerated T1 lines, strong 67-3 and weak 83-1 were selected for suppression of the endogenous cytosolic *G6PD* isoforms by supertransformation with a Xanthi-specific dsRNAi construct, which resulted in more uniform responses due to successful isoenzyme replacement (Scharte et al., 2009). Interestingly, the Arabidopsis enzyme of heterotrophic plastids in the cytosol (cP2) promoted both stress tolerance and development of the transgenic tobacco plants. In several

aspects, the Xanthi-cP2 lines reacted like the SNN cultivar, with respect to fast pathogen responses and earlier flowering, but also endured water stress better than the wild-type plants and produced more inflorescences (Scharte et al., 2009).

Here, we describe that improved performance of the Xanthi-cP2 lines correlates with metabolic priming by elevated fructose-2,6-bisphosphate (F2,6P<sub>2</sub>) levels. F2,6P<sub>2</sub> is a signalling molecule that regulates the direction of sugar-phosphate flux in the cytosol of eukaryotes, with an additional enzyme (reversible pyrophosphate:fructose-6-phosphate 1-phosphotransferase, PFP) for carbohydrate distribution in plant cells (reviewed by Stitt, 1987). Twofold elevated F2,6P<sub>2</sub> levels in the Xanthi-cP2 lines led to partial sugar retention, allowing for enhanced biosynthesis of fatty acids, and proline under salt stress.

## RESULTS

### Near-isogenic Xanthi-cP2 lines retain enhanced defence responses

During selfing of the isoenzyme-replaced Xanthi lines (cP2-67::cytRNAi and cP2-83::cytRNAi; Scharte et al., 2009), we noticed that pre-selection on sucrose-containing media influenced the soluble sugar levels in *source* leaves after transfer to soil (Figure S1). Thus, starting with super-transformed generation 4 (ST4, Figure 1a), seeds were directly sown on soil and raised in the greenhouse. In generation ST6, plants were transferred to climate chambers and challenged by *Phytophthora* zoospore infiltration. In the marked *source* leaf areas, the formation of ROS (Figure 1b) and callose (Figure 1c) was accelerated significantly, showing as twofold higher cell death rates compared with Xanthi wild type (Figure 1d). This finally resulted in the formation of necrotic lesions (Figure 1e) reminiscent of the hypersensitive (HR) response in pathogen-resistant *N. tabacum* cultivar SNN. Hence, the near-isogenic Xanthi-cP2 lines could be used for further analyses.

First, zoospore infiltration was repeated to measure phytohormone and metabolite levels linked to pathogen responses or stress priming (Baier et al., 2018; Hake & Romeis, 2019). Time-resolved analyses of water- versus zoospore-infiltrated *source* leaves showed that the Xanthi-cP2 lines reacted similarly to parental Xanthi and not the SNN cultivar (Figure S2). This was the case for both JA (measured as mixture of jasmonoyl-leucine/jasmonoyl-isoleucine) and much later appearing SA (salicylic acid), as well as for ABA (abscisic acid) and ICA (indole-3-carboxylic acid) levels. ABA is an indicator for drought stress and ICA for immune-priming linked to callose formation (Gamir et al., 2018). The obtained results showed that the improved stress responses of the Xanthi-cP2 lines are likely due to metabolic adjustments.

### Elevated fructose-2,6-bisphosphate levels lead to partial sugar retention

Regarding carbohydrate distribution, cytosolic fructose-2,6-bisphosphate (F2,6P<sub>2</sub>) is known to fine-tune sucrose export versus sugar retention. Moreover, this signalling molecule has been linked to wounding and changed water status in plants (Stitt, 1987). We previously showed that 6-phosphogluconate (6PG) accumulates in the Xanthi-cP2 lines (Scharte et al., 2009), which may lead to an increase of F2,6P<sub>2</sub> via inhibition of the bi-functional enzyme 6-phosphofructo-2-kinase/fructose-2,6-bisphosphatase (F2KP; Figure 2c). F2,6P<sub>2</sub> levels were determined in *source* leaves of unstressed plants over the day, revealing about twofold elevated amounts in the Xanthi-cP2 lines compared with Xanthi wild type (or SNN; Figure 2a). In zoospore-infiltrated SNN leaves, F2,6P<sub>2</sub> raised to similarly high amounts over time (Figure 2b), resulting in sugar retention and stimulated flux through the OPPP (Scharte et al., 2005, 2009).

### Assimilate partitioning is shifted towards a higher share of lipids

To check for F2,6P<sub>2</sub>-mediated sugar accumulation, we measured carbohydrate contents of mature *source* leaves. Both soluble sugars (glucose, fructose and sucrose) and starch levels were markedly raised in the Xanthi-cP2 lines compared with Xanthi wild type (Figure 3a). Glucose-to-fructose ratios were elevated to 2.8 and 2.9 compared with 1.5 in Xanthi wild type and 2.3 in SNN (Figure 3b), indicative of partial hexose sequestration in vacuoles (Wingenter et al., 2010). Furthermore, the twofold higher hexose-to-sucrose ratios (0.6 in the Xanthi-cP2 lines compared with 0.3 in Xanthi and 0.5 in SNN) pointed to *sink*-type metabolic activity (Farrar, 1993; Moore et al., 1999). Of note, lipid contents were significantly increased in the transgenic lines (Figure 3c), with unaffected protein levels compared with Xanthi wild type (Figure 3d). Thus, assimilate partitioning appeared altered in non-stressed plants of the Xanthi-cP2 lines, wherefore overall growth parameters were determined next.

### Biomass is mainly allocated to inflorescences and seeds

Plant height and biomass of above-ground tissues of the Xanthi-cP2 lines lay in between susceptible Xanthi and resistant SNN, with little differences in total leaf number (Figure 4a). Plants of the Xanthi-cP2 lines flowered about 1-week earlier—along with SNN, as reported earlier (Scharte et al., 2009), possibly due to elevated soluble sugar levels in *source* leaves, which is known to promote flowering (reviewed in Cho et al., 2018). In accordance, assimilates were mainly allocated to inflorescences as opposed to leaves or stems (Figure 4b), resulting in higher seed yields (about 15–20%)—which by trend were also maintained under drought stress (100% versus 50% water,

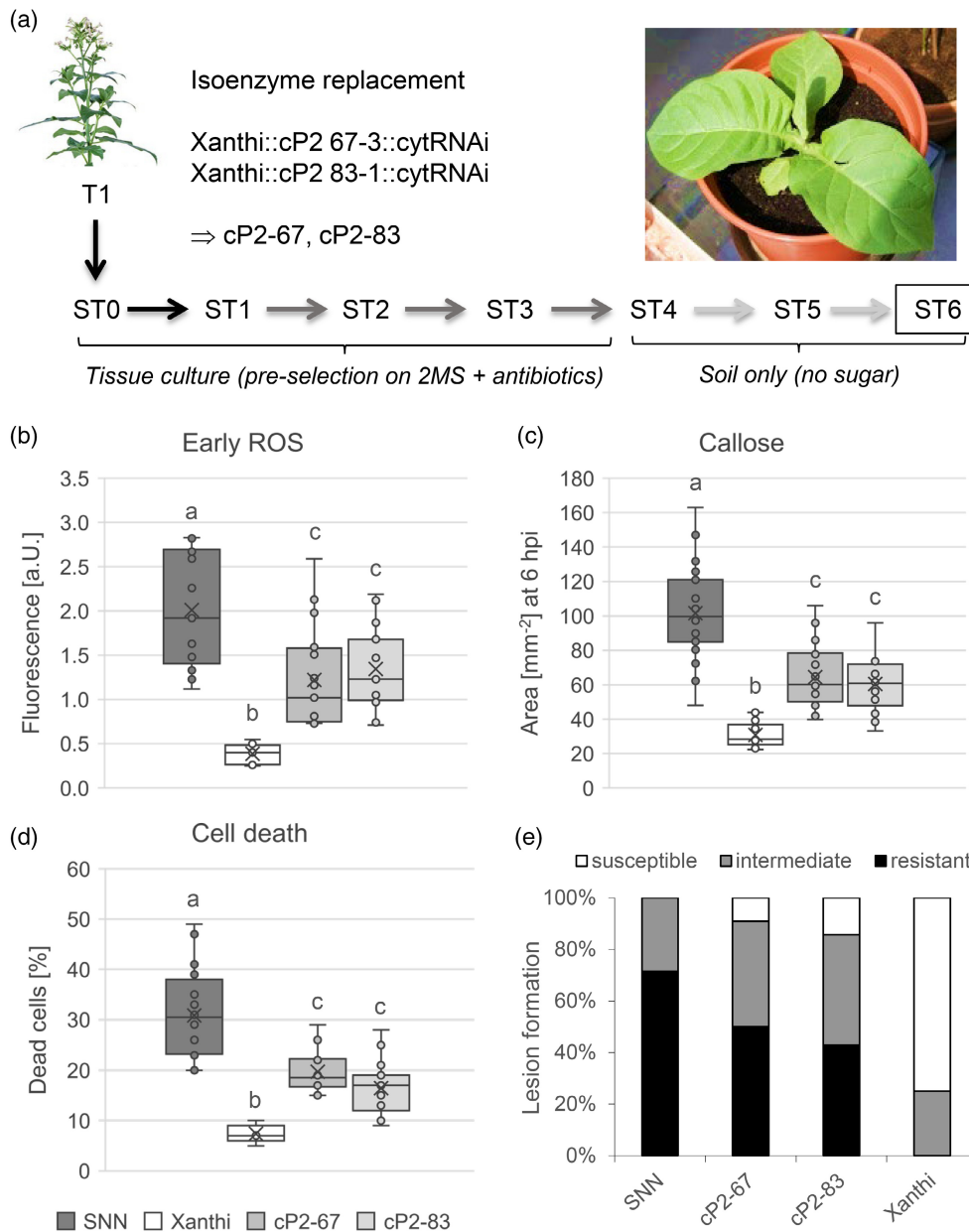


**Figure 1.** Biotic stress parameters persist in the near-isogenic Xanthi-cP2 lines.

*N. tabacum* var. Xanthi lines, expressing a cytosolic version of *A. thaliana* *G6PD3* under control of the Cauliflower mosaic virus 35S promoter, were characterized in the T1 and lines cP2-67 and cP2-83 super-transformed (ST) with a *cytG6PD*-RNAi construct (cP2::cytRNAi; Scharte et al., 2009).

(a) The progeny was pre-selected on MS medium with 2% sucrose and antibiotics until the ST3 generation (grey arrows). Starting with the ST4, seeds were directly sown on soil (light grey arrows) and subjected to various analyses in the following generations (ST5 to ST6).

(b) ROS formation 15 min after *Phytophthora nicotianae* infiltration (DFC fluorescence, a.u. arbitrary Units);  $n \geq 4$  replications.

(c) Callose deposition at plasmodesmata 6 h post-infiltration (hpi);  $n \geq 4$  replications.

(d) Cell-death rates;  $n \geq 6$  replications. Data were compiled in Excel with box plots showing the mean (x), the median (line) and outliers (dots outside boxes). Different statistical groups ( $P < 0.05$ ) are indicated by letters (one-way ANOVA with Tukey's post hoc test).

(e) Lesion formation in source leaves after zoospore infiltration;  $n \geq 6$  replications with Samsun NN (SNN) as HR wild-type control.

Figure S3). Seeds of well-watered plants were analysed for stored ingredients, that is carbohydrate (CHO), protein and lipid contents, revealing significantly elevated thousand-grain weights (Figure 5a) with seed composition shifted to a higher share of lipids—mainly at the expense of stored

starch (Figure 5, panels b and d). The higher lipid-to-CHO ratio of the Xanthi-cP2 lines (0.7 compared with 0.5 of Xanthi and 0.6 of SNN; Figure 5c) showed that *G6PDH*-isoenzyme replacement increases the energy density of seeds.

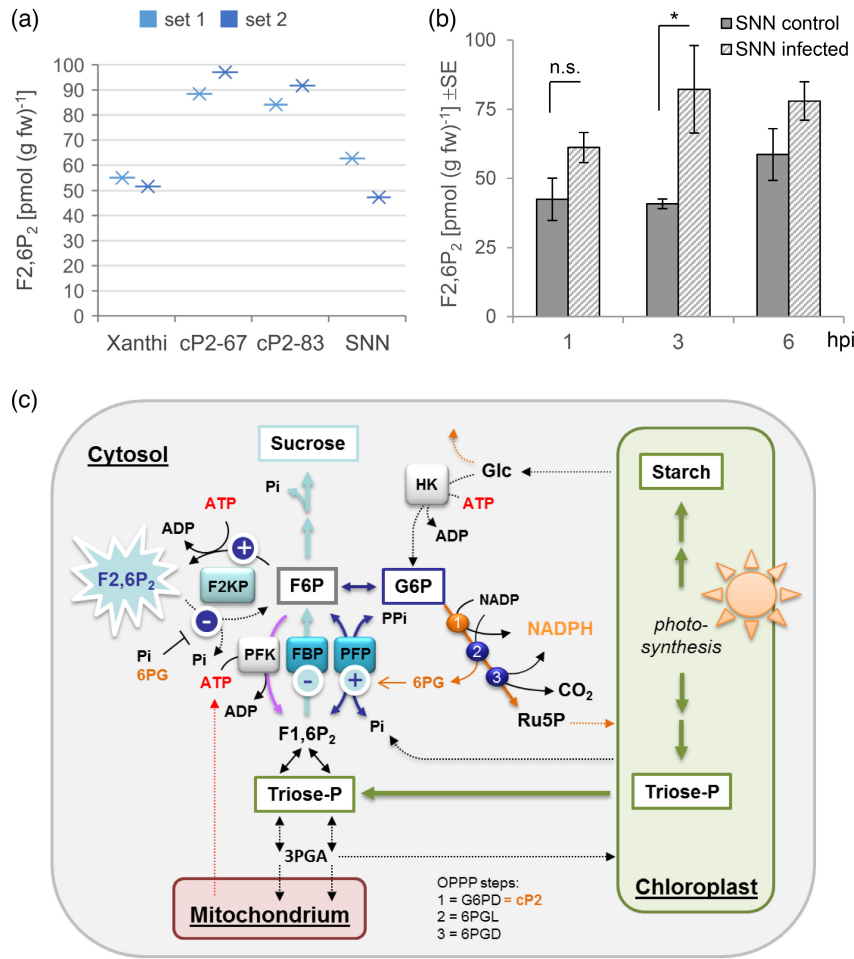


**Figure 2.** Leaves of the Xanthi-cP2 lines contain about twofold elevated F<sub>2,6</sub>P<sub>2</sub> levels.

(a) Fructose-2,6-bisphosphate (F<sub>2,6</sub>P<sub>2</sub>) contents in *source* leaves (four plants per genotype). Data represent mean values (over the day) of two replications (sets). (b) F<sub>2,6</sub>P<sub>2</sub> levels in water-infiltrated (control) versus zoospore-challenged SNN leaves (hpi, hours post-infiltration). Bars represent the mean ( $\pm$ SE) of three replications. Significant differences are indicated by a star ( $P < 0.05$ ); n.s., not significant. Note that in non-stressed leaves of the Xanthi-cP2 lines, F<sub>2,6</sub>P<sub>2</sub> levels were about twofold of Xanthi wild type and resemble those of zoospore-infected SNN (3–6 hpi).

(c) Scheme modified according to Nielsen et al. (2004). Note that the phosphatase reaction of bi-functional F2KP (6-phosphofruktose-2-kinase/fructose-2,6-bisphosphatase) can be inhibited by either Pi or 6-phosphogluconate (6PG) (dark blue sphere with white minus sign), wherefore elevated 6PG levels in the Xanthi-cP2 lines (Scharte et al., 2009) lead to elevated F<sub>2,6</sub>P<sub>2</sub> levels (light blue flash sign). High F<sub>2,6</sub>P<sub>2</sub> attenuates sugar export via inhibition of unidirectional FBP (fructose-1,6-bisphosphatase, light blue sphere with blue minus sign), favouring flexible use of carbohydrates via activation of PFP (reversible pyrophosphate:fructose-6-phosphate 1-phosphotransferase, light blue sphere with blue plus sign). HK, hexokinase; PFK, Phosphofruktokinase; Triose-P, triose phosphates (dihydroxyacetone phosphate = DHAP and glyceraldehyde 3-phosphate = GA3P). The three OPPP enzymes are indicated by numbers, with consequences of G6PDH-isoenzyme replacement by a cytosolic P2 isoform ( $K_{i[NADPH]} > K_{m[NADP+]}$ ) depicted in orange.

### Seedlings and mature leaves show improved abiotic stress tolerance

To test for elevated abiotic stress tolerance, salt and drought stress conditions were mimicked during seedling establishment and root growth by raising the concentration of NaCl or mannitol in agar media. Germination rates, relative to the non-stressed condition, revealed much better performance of the Xanthi-cP2 lines compared with Xanthi wild type, with similar results obtained at equivalent osmotic pressure (Figure 6a,b, comparing 150 mM NaCl to 300 mM mannitol). On vertical hard agar plates,

primary root lengths on 200 mM NaCl resembled those on 300 mM mannitol (as reported by Udawat et al., 2016), with growth rates of the Xanthi-cP2 lines similar to Xanthi wild type (Figure 6c). On MS control and 150 mM NaCl plates, cP2-67 performed similarly well—but remained shorter, which may be linked to about 20% wider roots compared with cP2-83 or Xanthi wild type (Figure S4a). Root growth ceased beyond 300 mM NaCl (not plotted) and little was recorded beyond 400 mM Mannitol.

Abiotic stress tolerance was also tested with excised leaf disks of non-stressed plants. No major differences

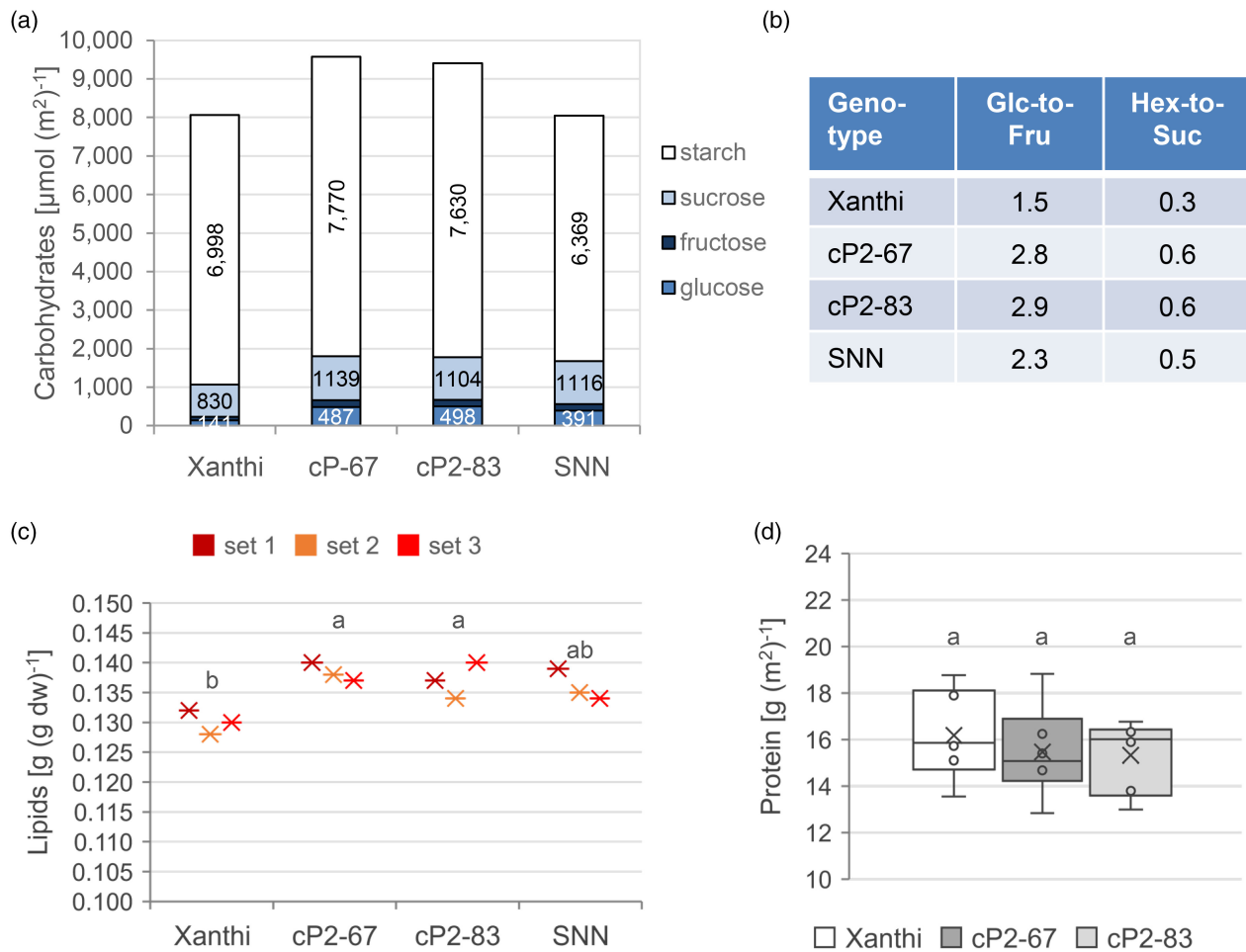


**Figure 3.** Sugar retention in *source* leaves leads to alter assimilate partitioning.

(a) Carbohydrate contents, of glucose (Glc), fructose (Fru), sucrose (Suc) and starch in *source* leaves of 3-week-old Xanthi-cP2 lines compared with Xanthi wild type and SNN (four plants per genotype).

(b) Soluble sugar ratios are indicative of subcellular localization: Glc-to-Fru ratios around 1 of cell-wall invertase activity, high Fru over Glc levels (up to 40-fold) of cytosolic invertase activity, and two- to fourfold higher Glc-to-Fru levels of vacuolar invertase activity (Wingenter et al., 2010). The hexose (Hex)-to-Suc ratio is a reliable parameter of *sink* strength (or metabolism; Moore et al., 1999). Note that the ratios of the Xanthi-cP2 lines lie about twofold higher compared with Xanthi wild type (and exceed those of SNN).

(c) Leaf lipid contents; (D) Leaf protein contents. Data ( $\geq 3$  replications) were compiled with Excel. For better visualization, the y-axis in panels c and d does not start at zero. The box plot of panel d shows the mean (x) and the median (line). Different statistical groups ( $P < 0.05$ ) are indicated by letters (one-way ANOVA with Tukey's post hoc test).

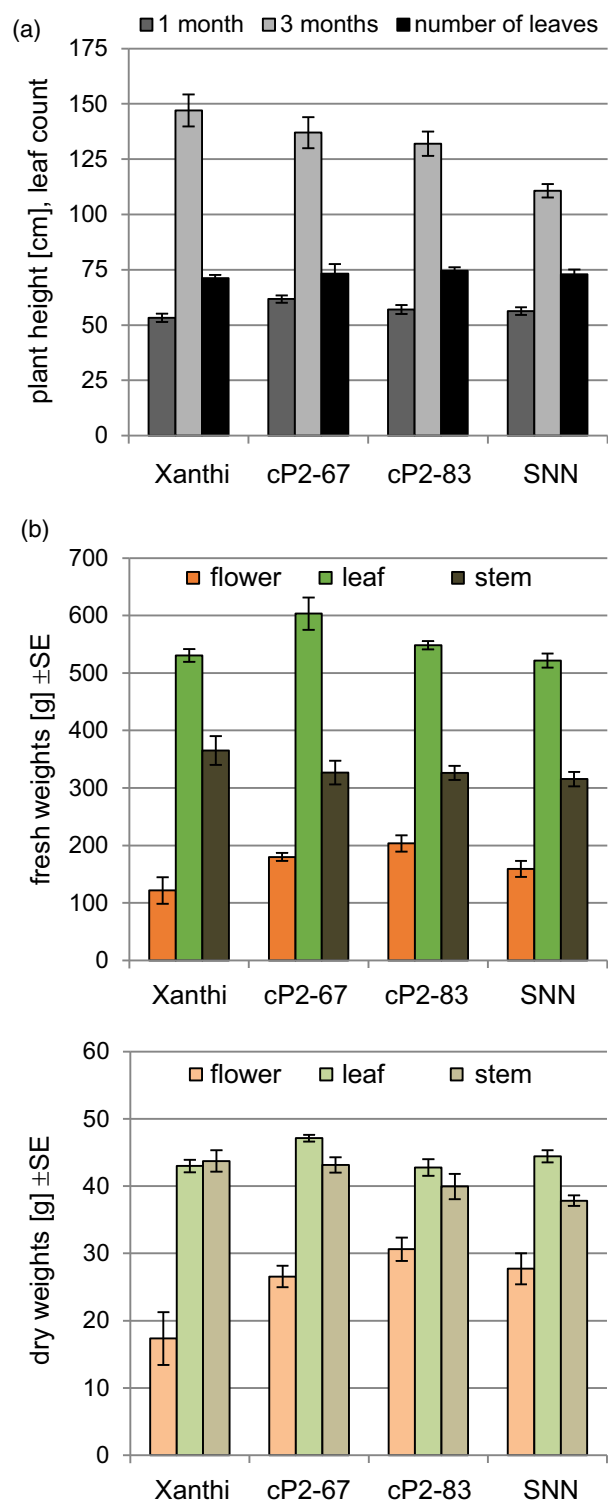
were detected upon raising the concentration of Methylviologen (MV = Paraquat) in the light (Figure S4b), causing ROS formation mainly in chloroplasts. Yet, leaf disks of the Xanthi-cP2 lines tolerated higher salt concentrations than Xanthi wild type (Figure S4c). Aside from elevated soluble sugar contents (see above), this may also result from higher proline levels, which was investigated next.

#### Salt stress leads to higher proline synthesis and efficient NADP(H) recycling

In most plants, stress tolerance of photosynthetic tissues correlates with an elevation of the compatible solute proline that can alleviate ROS formation by contributing to

NADP<sup>+</sup> recycling (reviewed in Alvarez et al., 2022). First,  $\delta^1$ -pyrroline-5-carboxylate reductase (P5CR) was enriched from crude leaf extracts of tobacco wild-type plants by anion-exchange chromatography (Figure S5a) and tested for preferred activity with NADPH (versus NADH) in the presence of salt (NaCl) or proline (Figure S5, panels b and c) as previously shown for Arabidopsis (Giberti et al., 2014), rice (Forlani et al., 2015) and barrel clover (Ruszkowski et al., 2015). Then, total amino acids, proline and NADP(H) contents were determined in *source* leaves of untreated and NaCl-treated plants (Figure 7).

In leaves of untreated plants, no major differences were found between Xanthi wild type and the transgenic



lines. Both, proline (Figure 7a) and total amino acids (Figure S6) increased during illumination, paralleled by elevated NADP(H) contents (Figure 7b). After watering plants with 150 mM NaCl for 2 days, proline raised 10-fold and amino acids threefold in all genotypes (Figures 7 and S6,

**Figure 4.** Growth parameters and biomass of above-ground plant parts. (a) Plant height in the greenhouse (at 1 month and at 3 months) aside from final leaf number counted for Xanthi wild type, the Xanthi-cP2 lines and SNN wild type. (b) Fresh and dry weights of the indicated tissues were determined at maturity of four plants per genotype with two replications. Bars represent mean values ( $\pm$ SE). Differences between the genotypes were not significant ( $P > 0.05$ ). Note that biomass of the Xanthi cP2 lines lay in between Xanthi wild type and SNN, with preferential allocation to inflorescences (flower) noticed previously (Scharte et al., 2009).

compare y-axis in panels a and c), confirming a specific raise of proline during salt stress. In the Xanthi-cP2 lines, proline accumulated to much higher amounts compared with fairly constant levels in Xanthi wild type (Figure 7c). This trend was also observed for the other amino acids, albeit to lesser extent (Figure S6c). NADP(H) contents of the NaCl-treated Xanthi-cP2 plants differed most significantly from Xanthi wild type between 2-h and 4-h illumination (Figure 7d). Concomitantly, NADPH/NADP<sup>+</sup> ratios showed the lowest values in this time period and a much later return to the initial levels (Figure S6d), indicative of higher NADPH consumption and recycling to NADP<sup>+</sup> in the transgenic lines.

#### Reduced sucrose export and enhanced PSII-induction kinetics

To study assimilate export, *source* leaves were harvested from greenhouse plants after 2-h illumination and transferred to a growth chamber. Leaf tips were trimmed and phloem exudates collected over a 6-h light and after an additional 16-h dark period (Figure 8a, top). In accordance with partial sugar retention (described above), sucrose efflux was reduced by about 10% in the Xanthi-cP2 lines (Figure 8a, bottom). Next, photosynthetic electron transport rates (ETR) were measured in greenhouse plants using a portable PAM fluorimeter. *Source* leaves of the Xanthi-cP2 lines showed enhanced PSII-induction kinetics (Figure 8b, left), with little differences at the stationary phase (Figure 8b, right). Considering the higher seed yields with elevated lipid-to-CHO ratios (described above), these results indicated that assimilates produced in *source* leaves of the Xanthi-cP2 lines reach *sink* tissues in altered composition.

#### Phloem exudates of the Xanthi-cP2 lines contain a higher share of lipids

Further experiments were conducted to determine amino acid and fatty acid contents in leaf exudates. An experiment conducted in winter (series 1) revealed that efflux during the day versus the night did not differ much for amino acids or proline (Figure 9a, top), but rather for fatty acids (Figure 9a, bottom). Efflux was highest during the day, for both long-chain fatty acids (LCFAs, C16 and C18) and very-long-chain fatty acids (VLCFAs, C20 and higher).

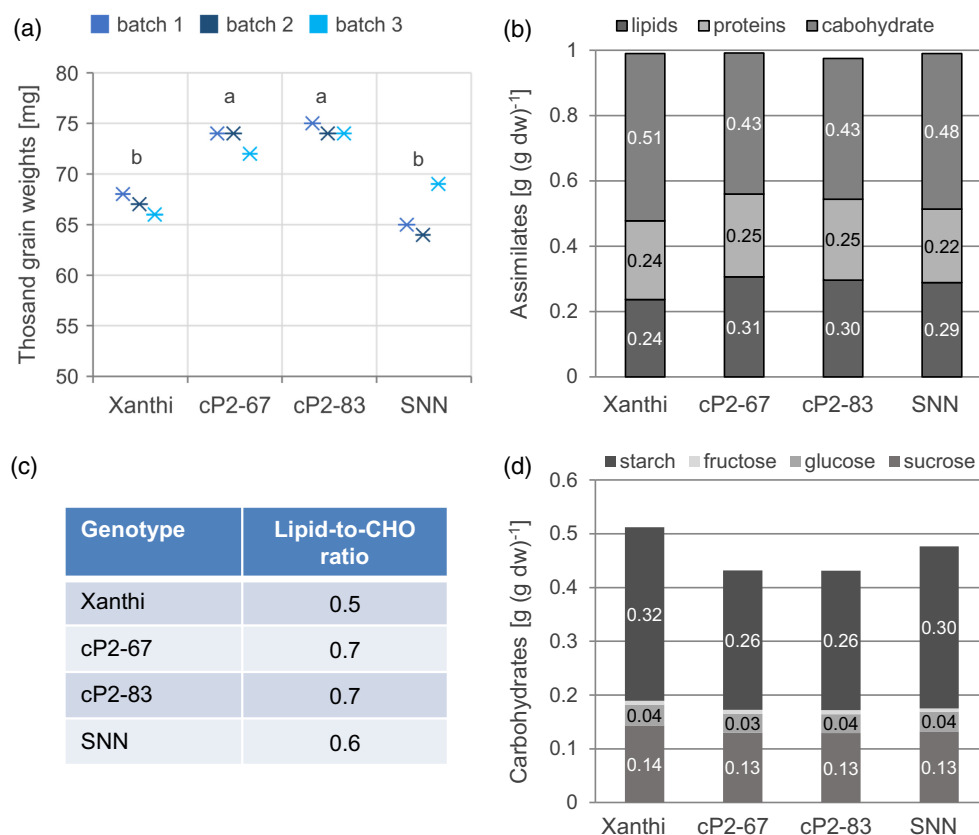


**Figure 5.** Higher seed yields with elevated thousand-grain weights and lipid contents.

(a) Thousand-grain weights of dry seeds (four plants per genotype) were determined with an automatic seed counter. Data represent the mean of three replications (batches). Note that the y-axis does not start at zero. Differences between the Xanthi-cP2 lines and Xanthi wild type were significant ( $P < 0.5$ ) as indicated by different letters (one-way ANOVA with Tukey's post-hoc test).

(b) Distribution among assimilates stored in seeds: carbohydrates (CHO), proteins and lipids; dw, dry weight.

(c) Lipid-to-CHO ratios (based on data in panel b). Note that the Xanthi-cP2 lines score higher than Xanthi wild type (and SNN).

(d) Carbohydrate composition of seeds. Lower contents of the Xanthi-cP2 lines compared with Xanthi wild type (in panels b and d) mainly correlate with a reduction in starch but also sucrose.

Total efflux of amino acids was similar for all genotypes, with slightly higher proline levels in SNN compared with Xanthi (Figure 9B, left). Total LCFA efflux from the Xanthi-cP2 lines was significantly higher (about threefold for cP2-67 and twofold for cP2-83) compared with Xanthi wild type, and by trend also that of VLCFAs (Figure 9b, right). This was even more evident for individual fatty acids, with 16:0 and 18:0 being the most abundant species in phloem exudates (Figure 9c). Interestingly, fatty acid composition of leaf disks (harvested from the same source leaf used for collecting exudates) was similar for all genotypes—with VLCFAs below the detection limit (Figure 9c, insert). This confirmed that linolenic acid (18:3) is the most abundant fatty acid in vascular plants (Mei et al., 2015, and references cited therein). Yet, 18:3 ranged low in the phloem exudates, demonstrating that lipid efflux occurs mainly in saturated form (as in Canola; Madey et al., 2002). Of note, oleic acid (18:1, preferentially bound by the Arabidopsis flowering locus T protein *in vitro*; Nakamura et al., 2014,

2019) was increased about twofold in phloem exudates of the Xanthi-cP2 lines (15 and 16 ng ml<sup>-1</sup> compared with 7 ng ml<sup>-1</sup> of Xanthi wild type), exceeding the levels of SNN (10 ng ml<sup>-1</sup>).

Repetitions in two greenhouse compartments in summer, with series 2 under regular (24°C day/20°C night  $\pm 2^\circ\text{C}$ ) and series 3 under 6°C colder growth conditions (18°C day/14°C night  $\pm 2^\circ\text{C}$ ), showed that more lipids are synthesized under regular conditions (Figure S7a, green). Series 1 (orange) resembled series 3 (blue) under colder growth conditions, also with respect to fatty acid levels detected in leaves (Figure S7, panels b and d). By trend, amino acid and fatty acid efflux was increased under colder growth conditions (Figure S8).

## DISCUSSION

In this study, we found that the basis for better performance of *N. tabacum* var. Xanthi plants with engineered G6PDH-isoenzyme replacement (Scharte et al., 2009) is



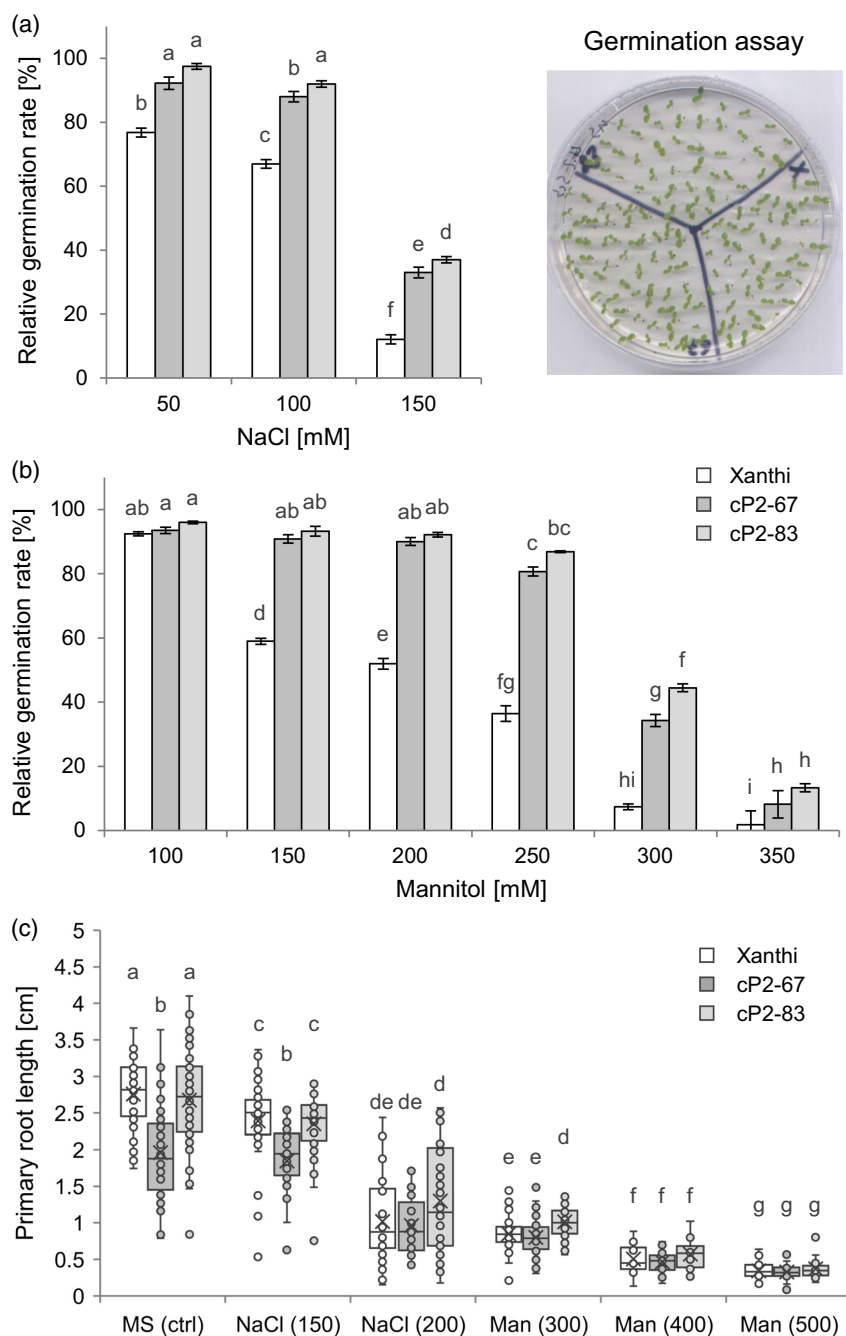


**Figure 6.** Salt versus drought stress during seedling establishment and root growth.

(a,b), About 40–50 seeds of the Xanthi-cP2 lines and Xanthi wild type were placed in sectors of the same agar plate for monitoring germination in the presence of salt (NaCl), or conditions mimicking drought stress (Mannitol). Bars show the mean ( $\pm$ SE) of three replications relative to the non-stressed condition for each genotype (MS control, 100%).

(c) For root growth analyses, surface-sterilized seeds were germinated on hard agar plates (MS control) in vertical position. After 1 week, the seedlings were transferred to square plates with MS control (ctrl) or the indicated NaCl (mM) or Mannitol (Man, mM) concentrations. Primary root growth was scored between Day 7 and Day 11 after transfer (three replications with 16 plants per genotype and condition,  $n = 48$  total). Note that on MS control plates, roots of cP2-67 plants were about 20% wider compared with cP2-83 and Xanthi wild type (Figure S4a). Data were compiled in Excel with box plots showing the mean ( $\bar{x}$ ), the median (line) and outliers (dots outside boxes). Different statistical groups ( $P < 0.05$ ) are indicated by letters (one-way ANOVA with Tukey's post hoc test and non-parametric statistics in panel c).

metabolic priming. Pathogen challenge of near-isogenic Xanthi-cP2 plants showed that stress-related hormone or metabolite profiles resemble susceptible Xanthi and not

the resistant tobacco cultivar SNN, hinting at mainly metabolic changes in the transgenic lines. In fact, F2,6P<sub>2</sub> levels were elevated about twofold in *source* leaves of

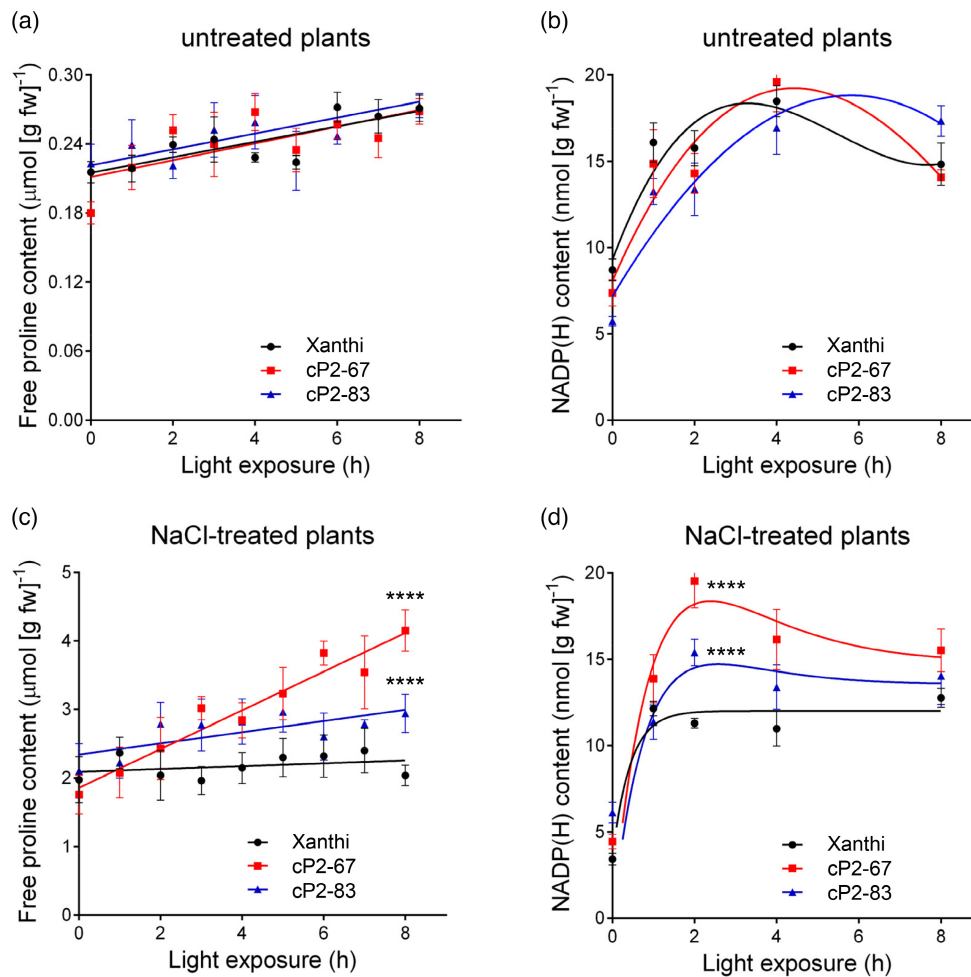


**Figure 7.** Higher proline and NADP(H) contents in leaves salt-stressed plants.

Plants of Xanthi wild type and the Xanthi-cP2 lines were incubated with water (untreated) or salt (150 mM NaCl) for 2 days. Untreated plants of all genotypes produced about similar free proline (panel a) and NADP(H) (panel b) during the light phase. After NaCl treatment, proline raised about 10-fold in all genotypes (compare the y-axis in panels a and c). Proline contents remained constant in Xanthi wild type during the light phase, but raised markedly in the Xanthi-cP2 lines (c), by about 40% in cP2-83 and 130% in cP2-67. A similar trend was found for the NADP(H) contents (d). Data points represent mean values ( $\pm$ SE) of six independent replications; \*\*\*\* $P < 0.0001$  (two-way ANOVA). For results on total amino acid contents and the NADPH/NADP<sup>+</sup> ratios, see Figure S6.

non-stressed Xanthi-cP2 plants, similar to those in SNN upon zoospore infiltration. Further analysis confirmed partial sugar retention and altered assimilate partitioning. Although vegetative biomass of the Xanthi-cP2 lines was comparable to Xanthi wild type, flowering started about 1-week earlier (along with SNN; Scharte et al., 2009). Concomitantly, assimilates were mainly allocated to reproductive tissues, although the CaMV-35S promoter (driving the transgenes) is less well expressed there (Wilkinson et al., 1997), which indicated that *source* leaves play a major role for the repeatedly elevated harvest yields. Indeed, under standardized growth conditions, seed mass obtained from the Xanthi-cP2 lines lay about 10–20% higher compared with Xanthi wild type—by trend also under water deprivation. Considering that thousand-grain weights and lipid-to-CHO ratios were increased,

G6PDH-isoenzyme replacement seems to affect both the *source* and *sink* tissues.

An important role of *sink* strength for photosynthetic performance under elevated CO<sub>2</sub> and nitrogen availability was found for tobacco plants grown under field conditions (Ruiz-Vera et al., 2017). Moreover, plants that are able to maintain both *source* and *sink* strength under drought tend to be more stress-resilient and productive (Rodrigues et al., 2019). Abiotic stress tolerance was clearly improved in the Xanthi-cP2 lines (Scharte et al., 2009, and this work), which has also been reported for the sole overexpression of cytosolic *G6PD* isoforms in other plant species (Yang et al., 2019; Zhao et al., 2020, and references cited therein).

Another obvious process that contributes to elevated stress tolerance in plants is the biosynthesis of proline as a universal abiotic stress marker (Alvarez et al., 2022; Ghosh

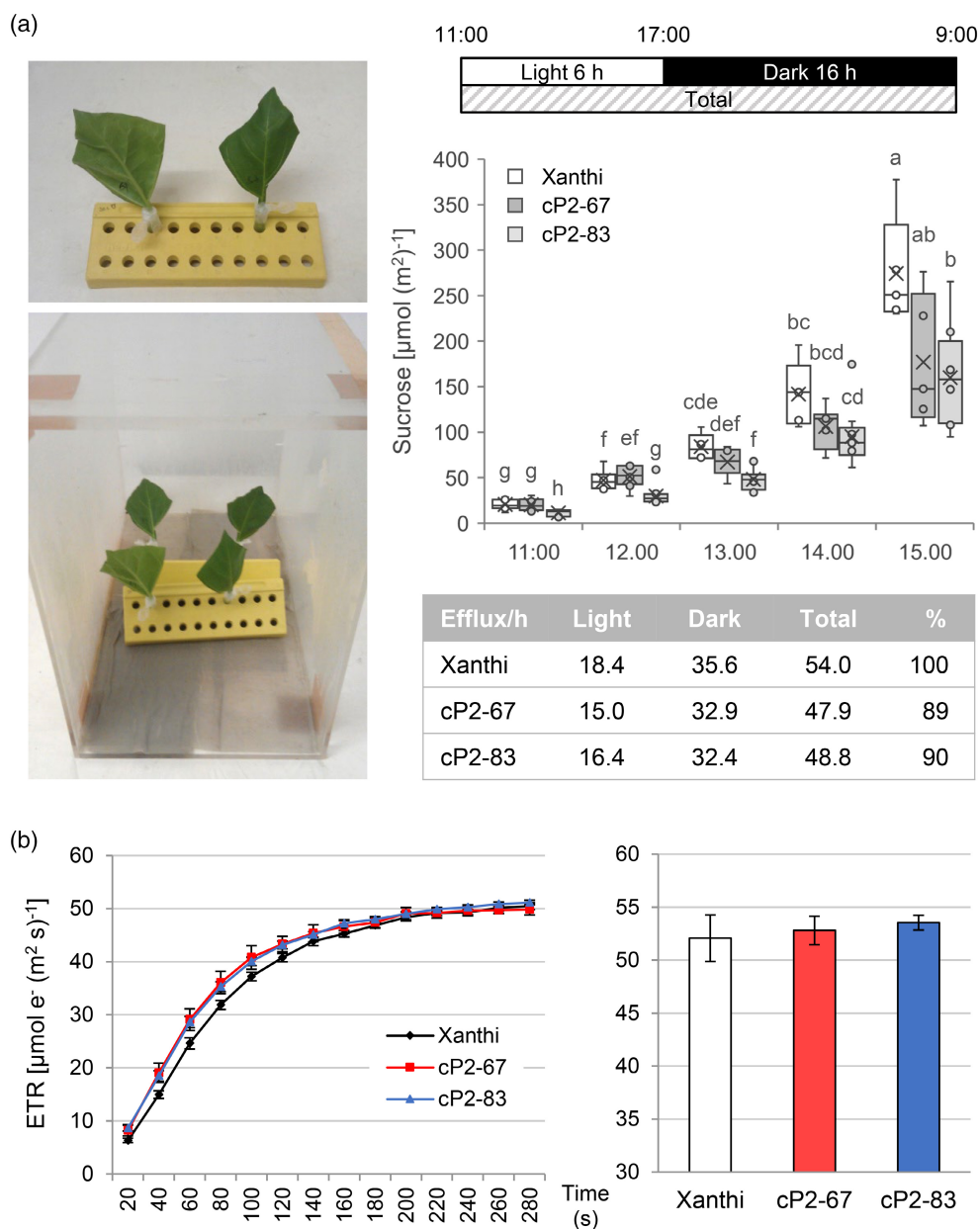


**Figure 8.** Reduced sucrose efflux and enhanced PSII-induction kinetics.

(a) Left, leaf 'flag' cuttings were placed in 15 mM EDTA solution and incubated in a translucent chamber. Right, a 6-h light phase was followed by a 16-h dark phase (top). Sucrose efflux was determined at the indicated time points and per cent efflux rates were calculated for the light and dark periods, differing by about 10% for the Xanthi cP2 lines from Xanthi wild type in total. Data were compiled in Excel with two plants per genotype and three replications. The box plots show the mean (x), the median (line) and outliers (dots outside boxes). Different statistical groups ( $P < 0.05$ ) are indicated by letters (two-way ANOVA with Tukey's post hoc test).

(b) Electron transport rates (ETR) were measured in *source* leaves of plants in the greenhouse over 5 min using a portable PAM fluorimeter. By trend, the Xanthi-cP2 lines showed enhanced PSII-induction kinetics, with little variation at the stationary phase ( $>240$  sec, saturation curves) or illumination with  $280 \mu\text{E}$  for 6 h at ambient  $\text{CO}_2$  (bar diagram). Data are the mean ( $\pm$ SE) of nine independent replications. Differences between the Xanthi-cP2 lines and Xanthi wild type were not significant ( $P > 0.05$ ).

et al., 2022). Overexpression of the key enzyme  $\delta^1$ -pyrroline-5-carboxylate synthetase (P5CS) in tobacco resulted in enhanced flower development and higher root biomass (Kishor et al., 1995). But unlike F2,6P<sub>2</sub>, proline levels were not altered in non-stressed plants of the Xanthi-cP2 lines.

Their basic stress tolerance is likely due to an elevation of soluble sugars (see Ingram & Bartels, 1996) with hexoses being partially sequestered in vacuoles (this work). Under salt stress, the Xanthi-cP2 lines accumulated more proline in *source* leaves during the light phase, which was

accompanied by elevated NADP(H) levels and efficient NADPH-to-NADP<sup>+</sup> turnover. Although the method used does not distinguish between cytosolic and plastidic NADP(H) pools, proline biosynthesis profits from elevated NADPH provision in the cytosol, since PC5S strictly

requires NADPH, and PC5R prefers NADPH over NADH in the presence of NaCl or proline (Giberti et al., 2014, this work). Of note, salt-induced proline biosynthesis in the light is governed by bZIP transcription factor HY5 in Arabidopsis, leading to elevated PC5S levels (proline

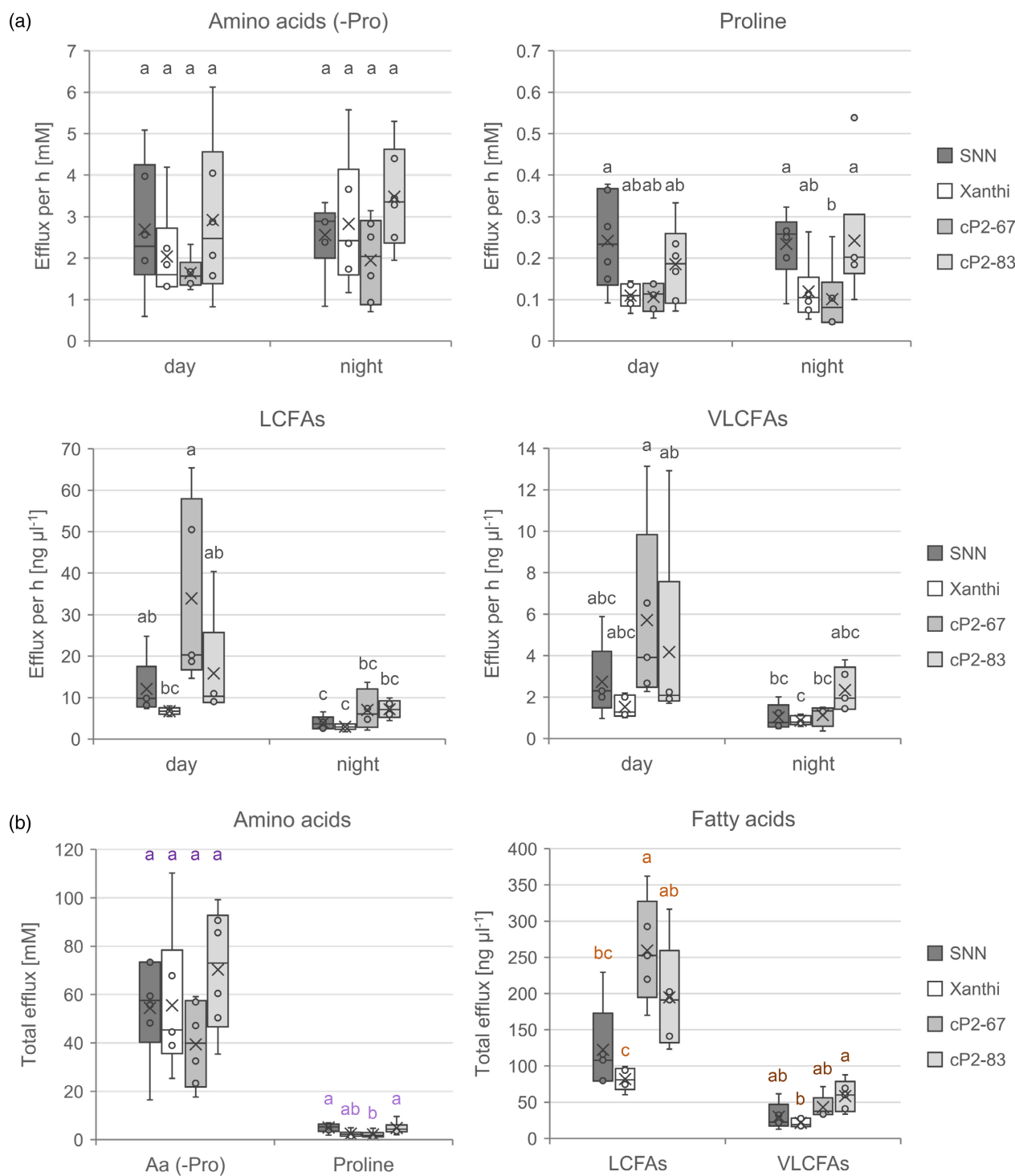
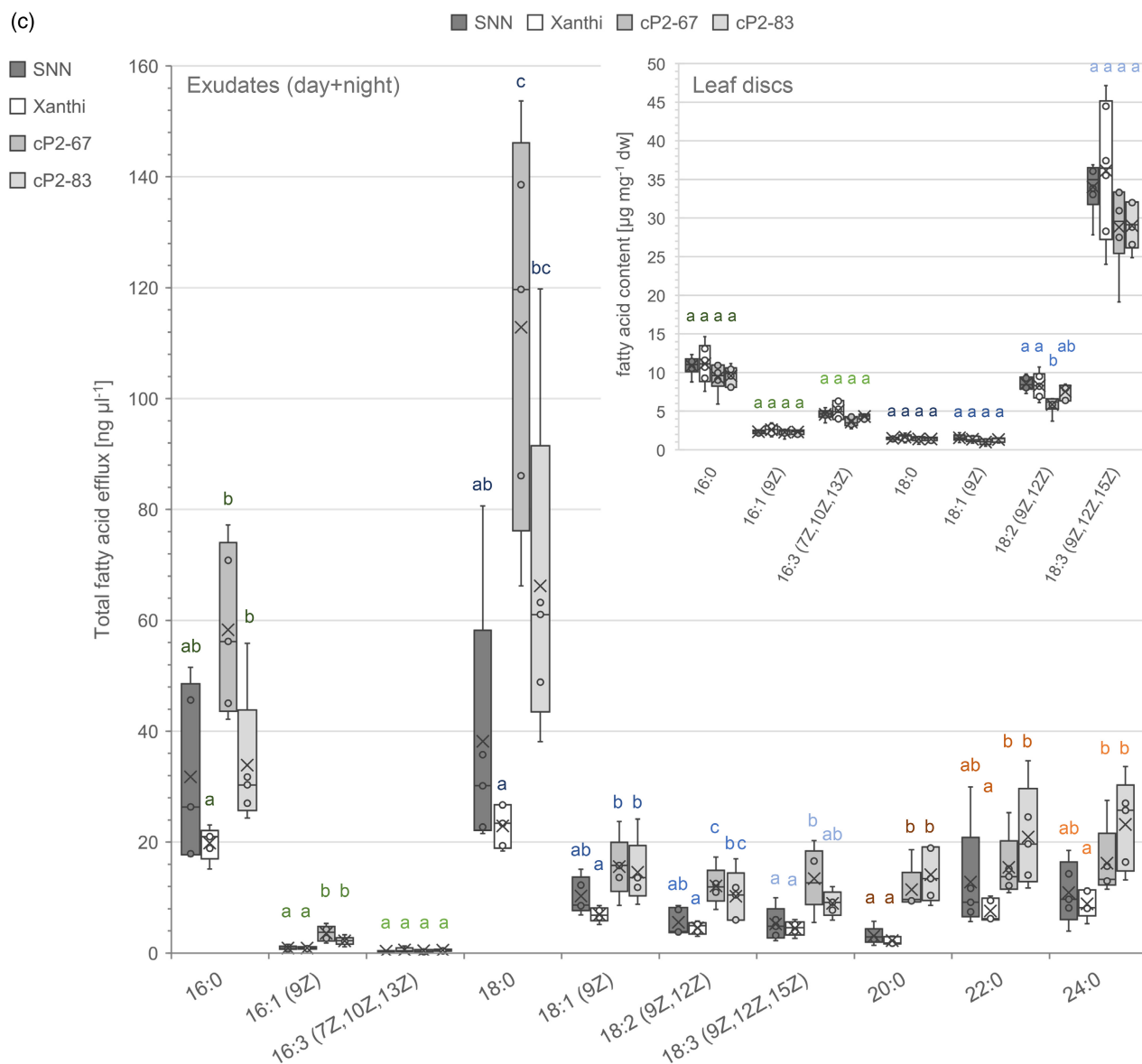


Figure 9. (Continued)



**Figure 9.** Phloem exudates of Xanthi-cP2 lines contain a higher share of fatty acids.

Plants in the greenhouse (grown under long day regime with additional illumination) remained smaller due to heating problems in winter, resulting in lower night temperatures. After transfer of *source* leaves to the laboratory, phloem exudates were collected over a 5-h light (day) and 16-h dark (night) period at 22–23°C.

(a) Amino acid efflux (top) and fatty acid efflux (bottom) per hour during the day versus the night.

(b) Total efflux over 21 h (day+night). Note that SNN tended to export more proline and the cP2 lines more fatty acids compared with Xanthi wild type. Aa, amino acids; Pro, proline; LCFAs, long-chain fatty acids (synthesized in plastids); VLCFAs, very-long-chain fatty acids (elongated at the ER).

(c) Fatty acid composition of phloem exudates versus leaf samples (insert), harvested from the central part of the same *source* leaf (six plants per genotype). Exudates (day+night) collected over 21 h contained mostly saturated LCFAs (16:0, 18:0), but also VLCFAs (20:0, 22:0, 24:0). Among the LCFAs, 18:1 (preferentially bound by the flowering locus T protein) accumulated to higher levels in the exudates of the Xanthi-cP2 lines compared with Xanthi wild type (exceeding the levels of SNN). Note that in leaf tissue (insert), 18:3 was the most abundant fatty acid, and VLCFAs were below the detection limit (dw, dry weight). Box plots (compiled in Excel) show the mean (x), the median (line) and outliers (dots outside boxes). In panels b and c, statistics were run for each character separately (colour-coded) with different groups indicated by different letters (one-way ANOVA with Tukey's post hoc test and non-parametric statistics).

biosynthesis) and lower PDH levels (proline catabolism; Kovács et al., 2019).

Anabolic pathways should generally profit from elevated NADPH provision—also when distributed across different compartments. After all, flux through the cytosolic

OPPP constantly feeds C5-sugar phosphates into the plastid stroma via metabolite transporters in the inner envelope membrane: Xu5P mainly by XPT (Eicks et al., 2002) and Ru5P also by GPT1 (Baune et al., 2020; for schemes see Linnenbrügger et al., 2022). Thus, the cP2 approach

impacts the complete PPP cycle in chloroplasts, showing as fast photosynthetic induction due to metabolic pools shared with the reversible reactions of the Calvin cycle (Scharte et al., 2009; this work). Pathways that withdraw metabolites from the PPP in plastids should therefore profit as well, especially the shikimate and phenylpropane pathway (starting from erythrose-4-phosphate in the stroma), extending to the biosynthesis of amino acids and fatty acids (this work), but probably also to nucleotides when needed in high amounts (e.g. during embryo development, Andriotis & Smith, 2019; Baune et al., 2020). Proline metabolism—distributed across the cytosol, plastids and mitochondria (reviewed in Szabados & Savouré, 2010)—mainly profited under stress (this work), being also intimately connected with fatty acid biosynthesis and redox metabolism in chloroplasts and mitochondria, as shown in *Arabidopsis* (Shinde et al., 2016).

Considering that the pathogen-resistant SNN cultivar did not tolerate water deprivation well (Scharte et al., 2009), sugar retention and enhanced PSII-induction kinetics, which is important under fluctuating light (shown for F2,6P<sub>2</sub>-deficient *Arabidopsis* mutants; McCormick & Kruger, 2015), alone—cannot explain all improvements in the Xanthi-cP2 lines. Rather, the combination of efficient NADP(H) recycling with little feedback inhibition by NADPH (cP2 enzyme) allowed to overcome limitations. Elevated carbohydrate levels not only provide ample energy (NADPH via the OPPP, ATP via glycolysis and respiration), but also serve as start material for most biosynthetic pathways. Thus, in agreement with elevated F2,6P<sub>2</sub> levels in *source* leaves of non-stressed Xanthi-cP2 plants, sucrose export was reduced and replaced by a higher share of fatty acids—especially in the light. The latter may reflect redox activation of acetyl-CoA carboxylase that catalyses the first committed step in the biosynthesis of long-chain fatty acids (16:0 and 18:0) in the stroma. After export from plastids, extension to very-long-chain fatty acids (C20 to C24) occurs at the cytosolic face of the ER, consuming NADPH in the cytosol together with desaturation by extra-plastidial FAD enzymes (Shanklin & Cahoon, 1998)—also indirectly, via ER-bound cytochrome P450 enzymes (Linnenbrügger et al., 2022; for reviews on lipid biosynthesis and transport in plants, see Li et al., 2016 and Rawsthorne, 2002). In fact, levels of polyunsaturated fatty acids (PUFAs, involving ER desaturases FAD2 and FAD3 in *Arabidopsis*; Lou et al., 2014) correlated with the growth rate of cell cultures from *Arabidopsis* and *Sycamore* (Mei et al., 2015). Yet, overexpression of a plastidial *G6PD* in the microalga *Phaeodactylum tricorutum*—supporting NADPH supply only in the stroma—increased fatty acid biosynthesis, but decreased that of VLCFAs (Xue et al., 2017). Besides LCFAs, also VLCFAs produced at the ER were significantly elevated in exudates of the Xanthi cP2 lines. They are important precursors of membrane lipids (e.g. sphingolipids) and may

also be stored in oil bodies as triacylglycerol (TAG). Being the precursors of cutin and wax, VLCFAs play important roles in plant responses to abiotic and biotic stress (reviewed in Batsale et al., 2021), with wax biosynthesis recently shown to improve drought tolerance in rice (Shim et al., 2023). On the other hand, phosphatidic acid (PA), an intermediate of lipid biosynthesis and important signalling molecule in plants (reviewed in Yu et al., 2017) may also contribute to improved stress responses in the transgenic lines. This possibility remains to be studied further.

Obviously, assimilates produced in the Xanthi-cP2 lines reach *sink* tissues in altered composition. Besides sucrose (and its derivatives, creating sufficient osmotic pressure in the phloem), also amino acids, hormones, inorganic acids, ions, micronutrients (e.g. vitamin C; Tedone et al., 2004), mRNA species, proteins and signalling molecules are co-transported—but also lipids. Evidence for fatty acid transport in the phloem was first reported for Canola (Madey et al., 2002) and occurs mostly in form of free fatty acids (saturated 16:0, 18:0), but also in bound form attached to electron-dense spherical particles in the phloem sap—and in much higher amounts when plants were stressed. In fact, LCFAs are fairly water-soluble (16:0 up to 7.2  $\mu\text{g } \mu\text{l}^{-1}$  and 18:0 up to 2.9  $\mu\text{g } \mu\text{l}^{-1}$  at 20°C; Ralston & Hoerr, 1942). By contrast, VLCFAs are insoluble in water and have to be transported entirely in bound form. Madey et al. (2002) stated that this resembles the long-distance transport of fatty acids in animals, bound to blood serum albumin (reviewed in Spector, 1975). In plants, they are passively co-transported with the bulk flow of sucrose, entering and leaving the phloem symplastically (via plasmodesmata between sieve tubes and companion cells). Upon arrival in *sink* tissues, unloading is likely driven by metabolic withdrawal—just like in the case of sucrose, amino acids and other substances co-transported in the phloem sap. In plant cells, catabolism and biosynthesis of fatty acids occur simultaneously (Kessel-Vigelius et al., 2013). Thus, upon activation (by acyl-CoA synthetases), they can enter peroxisomes for degradation ( $\beta$ -oxidation) and conversion to succinate (in the glyoxylate cycle). Succinate, shuttled back into the cytosol, is converted to pyruvate and may enter mitochondria for respiration or plastids for anabolic purposes. Alternatively, activated fatty acids may directly replenish the acyl-CoA pools at the cytosolic face of the ER, where NADPH-dependent chain elongation and TAG synthesis take place. TAG is stored in lipid droplets formed at the ER (reviewed in Ischebeck et al., 2020), and VLCFAs—as precursors of membrane lipids, cutin and wax (exported into the apoplast)—do not accumulate in leaf tissue (Li et al., 2016 and this work; Figure 9c, insert).

Proteomic analyses of *Arabidopsis* phloem exudates have identified candidate proteins linked to both lipid transport and signalling (Barbaglia et al., 2016; Guelette et al., 2012). In fact, phosphocholin (PC, diurnally

oscillating in leaves) seems to influence flowering in Arabidopsis by binding to the FT protein (transported in the phloem), preferentially as linoleic acid (18:1, Nakamura et al., 2014, 2019), also in tobacco (Beinecke et al., 2018). Hence, higher lipid efflux from *source* leaves in the Xanthi-cP2 lines, with significantly elevated LCFA and VLCFA levels, may not only promote earlier flowering—but partially compensate for the reduced sucrose export rates in the Xanthi-cP2 lines.

Regarding lipid production, Vanhercke et al. (2014) reported that engineering TAG biosynthesis in tobacco led to 15% higher lipid contents in leaves. Compared with this targeted approach, G6PDH-isoenzyme replacement resulted in 5% higher lipid contents in leaves and about 20% higher lipid contents in seeds of the Xanthi-cP2 lines—mainly at the expense of stored starch. Moreover, retention of soluble sugars should allow for the formation of trehalose-6-phosphate (T6P), which promoted fatty acid biosynthesis in Arabidopsis by stabilizing the transcription factor WRINKLED (Zhai et al., 2018). WRINKLED plays an important role in TAG biosynthesis during seed development, which seems to be conserved across plant species (Kuczynski et al., 2022), also upregulating genes encoding the third OPPP enzyme 6PG dehydrogenase (dual cytosolic/plastidic PGD1 and PGD3 in Arabidopsis; Hölscher et al., 2016). Yet, causative for altered assimilate partitioning in the Xanthi-cP2 lines are most likely the twofold elevated F<sub>2,6</sub>P<sub>2</sub> levels, leading to metabolic priming and sugar retention. Similar to phosphate (Pi), 6PG, accumulating in the cP2 lines (Scharte et al., 2009), inhibits the phosphatase reaction of bi-functional enzyme F2KP (6-phosphofructose-2-kinase/fructose-2,6-bisphosphatase; Villadsen & Nielsen, 2001). Elevated F<sub>2,6</sub>P<sub>2</sub> levels slow down sucrose export, both by inhibition of unidirectional FBPase (fructose-1,6-bisphosphatase, Figure 2c; light blue minus sign) and by activation of bi-directional PFP (pyrophosphate:fructose-6-phosphate 1-phosphotransferase, light blue plus sign). Higher metabolic flux via the OPPP (Figure 2c, highlighted in orange), combined with less feedback inhibition by high NADPH levels in the isoenzyme-replaced Xanthi-cP2 lines, should therefore allow for versatile use of the retained carbon skeletons. Due to bifunctionality of the F2KP enzyme (that may synthesize or destroy F<sub>2,6</sub>P<sub>2</sub>), this is difficult to achieve otherwise, because simple overexpression of F2KP would not work. G6PDH-isoenzyme replacement, however, bypasses the complex stress signalling network that was genetically fixed during plant evolution (Yu et al., 2017). Stress signalling is mainly coordinated by antagonistic action among phytohormones (Karasov et al., 2017; Leisner et al., 2022), which was not changed in the Xanthi-cP2 lines. Our analyses thus support that the energy limitation myth can be dismissed. Like in other organisms, evolution tries to avoid extinction and does not optimize energy-use efficiency (Maggio et al.,

2018). After all, plants rely on a resource (sunlight) that is diurnally available, with photosynthesis being mainly *sink*-limited by downstream metabolism (von Schaewen et al., 1990; Stitt et al., 1991; reviewed in Paul & Foyer, 2001).

Importantly, in the Xanthi-cP2 lines, several limitations were overcome, which obviously affected the *source-sink* interactions (see reviews by Chang & Zhu, 2017; Murchie et al., 2023). Sustained NADP(H) provision in the cytosol 'pushed' both stress responses and development by facilitating oxidative bursts and anabolic biosyntheses (mainly of fatty acids, but also amino acids—under stress specifically proline). Higher seed yields with elevated lipid contents obtained from the transgenic lines indicate that metabolism in *sink* tissues also profited ('pull'). Facilitated by accelerated flowering (due to elevated soluble sugar and linoleic acid levels) and stimulated fatty acid synthesis, the harvest index (seed per vegetative biomass) raised for the Xanthi-cP2 lines (approximately 1 compared with 0.77 of Xanthi and 0.7 of SNN), which is highly promising and should be repeated under fluctuating light conditions—ideally in the field.

Considering that low *sink* strength negatively affected tuber quality and yield in a heat-sensitive potato cultivar (Hastilestari et al., 2018), the cP2 approach may also improve stress tolerance and development in other *Solanaceae*. In fact, TAG turnover was recently shown to be required for efficient stomata opening during heat stress in Arabidopsis (Korte et al., 2023). Based on systems biology and metabolomic analyses, the establishment of a primed or pre-conditioned state has been suggested for improving crop plants (Tugizimana et al., 2018). Therefore, introduced in one step, using either a cP2-RNAi double construct or CRISPR/Cas9 for knock-in of a heterologous cP2 into the cytosolic G6PD loci (e.g. by the DOTI technique, see editorial of Sanchez-Muñoz, 2023), G6PDH-isoenzyme replacement could be easily tested for circumventing the genetically fixed growth/defence trade-off in other plant species.

## EXPERIMENTAL PROCEDURES

### Plant growth and harvest

Seeds of super-transformed Xanthi-cP2 lines (Scharte et al., 2009) were surface sterilized and pre-selected on solid Murashige & Skoog medium (MS salts plus vitamins, adjusted to pH 5.6 with KOH, 0.4% agar; Duchefa, Haarlem, NL) supplemented with 2% sucrose, and antibiotics (40 mg/L hygromycin, 100 mg/L kanamycin) after autoclaving. From generation ST4 on, seeds were directly sown on soil in the greenhouse and grown under long day regime with additional illumination (16-h light at 300–400  $\mu\text{mol quanta m}^{-2} \text{sec}^{-1}$ ). After 3–6 weeks, leaf disks of three to four plants per genotype were harvested from *source* leaves with a cork borer (two intercostal fields, opposite of the midrib) and frozen in liquid nitrogen. Prior to pathogen challenge, plants were transferred to a growth chamber (14-h light with 300–350  $\mu\text{mol quanta m}^{-2} \text{sec}^{-1}$ , 10-h dark) for 3-day acclimation.

Plant height was measured after 1 and 3 months (onset of flowering). At maturity, leaf number was counted prior to biomass analyses. Seeds were harvested from parallel plant sets and dried at RT for at least 2 weeks prior to storage/further use.

### Pathogen challenge and microscopic detection of ROS, callose and cell death

Infiltration of *Phytophthora nicotianae* (van Breda de Haan) into tobacco leaves was conducted as described previously (Essmann et al., 2008; Scharfe et al., 2005). Briefly, 1 h after the onset of light, intercostal fields of the same source leaf (on opposing sides of the midrib) were infiltrated with zoospores or water, circled with a water-resistant pen and kept under long day regime. At different time points, leaf disks were excised from the infiltrated areas with a cork borer and snap-frozen for metabolite analyses. For ROS detection, freshly harvested leaf disks were incubated in 10  $\mu\text{M}$  2',7'-dichlorodihydrofluorescein diacetate ( $\text{H}_2\text{DCF-DA}$ , Molecular Probes, Invitrogen) for 10 min. ROS-dependent oxidation of non-fluorescent  $\text{H}_2\text{DCF-DA}$  to highly fluorescent DCF was recorded at 488 nm excitation/500–535 nm emission with a confocal laser-scanning microscope (CLSM; TCS SP2, LEICA Microsystems GmbH, Wetzlar, Germany). Callose was stained with Aniline Blue according to Gómez-Gómez et al. (1999): The epidermal layer was peeled off and leaf disks were bathed in Farmer's fluid (3:1 Ethanol-acetic acid) for chlorophyll removal. After washing with water for 15 min, samples were incubated for 20 min in Aniline Blue solution (0.1% in 0.1 M  $\text{K}_2\text{HPO}_4$  pH 7). Fluorescent cells in a defined area were quantified with a conventional fluorescence microscope (DMRBE, Leica) using a 340–380 nm excitation filter, 400 nm dichromatic mirror and 425 nm barrier filter. High-resolution images were recorded with the CLSM at 405 nm excitation/510–520 nm emission. Cell death rates were determined upon infiltration of propidium iodide (0.5 mg  $\text{ml}^{-1}$ ) according to Curtis and Hays (2007). Intercalation into DNA of dead cells was documented with the CLSM at 488 nm excitation/590–650 nm emission, and chlorophyll fluorescence of living cells at 670–710 nm emission. Per plant, 33 images of four leaf areas were used to calculate the ratio of dead to living cells.

### Phytohormone analyses

Approximately 200 mg fresh weight of the same plant material as for the lipid analysis was extracted, similar to the procedure described for lipids in Matyash et al. (2008). Analysis was performed on an Agilent 1100 HPLC system (Agilent, Santa Clara, CA, USA) coupled to a hybrid triple quadrupole / linear ion trap mass spectrometer (Applied Biosystems 3200, Life Technologies, Carlsbad, CA, USA) as described (Ternes et al., 2011). Phytohormones were identified by multiple reaction monitoring (MRM) in negative ion mode. Mass transitions were as follows: 141/97 [declustering potential (DP) –45 V, entrance potential (EP) –7 V, collision energy (CE) –22 V] for  $\text{D}_4\text{-SA}$ , 137/93 (DP –45 V, EP –7 V, CE –22 V) for SA, 179/135 (DP –40 V, EP –6.5 V, CE –22 V) for  $\text{D}_5\text{-IAA}$ , 160/116 (DP –40 V, EP –6.5 V, CE –22 V) for ICA, 325/133 (DP –80 V, EP –4 V, CE –30 V) for  $\text{D}_3\text{-JA-Leu}$ , 322/130 (DP –80 V, EP –4 V, CE –30 V) for JA-Ile/Leu, 269/159 (DP –55 V, EP –9 V, CE –16 V) for  $\text{D}_6\text{-ABA}$  and 263/153 (DP –55 V, EP –9 V, CE –16 V) for ABA.

### Carbohydrate measurements

Total carbohydrate contents were determined as described in Essmann et al. (2008).

### Fructose-2,6-bisphosphate

Frozen leaf tissue was extracted under alkaline conditions (van Schaftingen & Hers, 1983) for determination of F2,6P<sub>2</sub> via activation of endogenous pyrophosphate: fructose-6-phosphate-1-phosphotransferase (as described in van Schaftingen et al., 1982). Snap-frozen leaf disks (1.8 cm in diameter) were ground in liquid nitrogen and resuspended in 0.5 ml of ice-cold 50 mM KOH. Samples were incubated for 60 min at 80°C in a water bath with occasional shaking. Then, a tip of spatula of activated charcoal was added, and samples were further incubated on ice for 20 min. After repeated centrifugation (16 000 g for 10 min at 4°C), the final supernatant was kept at 4°C and used within 24 h. F2,6P<sub>2</sub> was measured photometrically (endpoint method, as described by Stitt, 1990). Briefly, 5  $\mu\text{l}$  of supernatant (or 2 pmol F2,6P<sub>2</sub>, Sigma F7006) was added to 200  $\mu\text{l}$  reaction buffer (100 mM Tris-HCl pH 8, 1 mM  $\text{MgCl}_2$ , 0.15 mM NADH, 0.25 mM F6P and 0.1 mg  $\text{ml}^{-1}$  NaPPI) in a microtiter plate reader (Tecan Safire). After recording blanks at 340 nm (3–5 cycles), reactions were started by adding 5  $\mu\text{l}$  of enzyme master mix (1 mM  $\text{MgCl}_2$ , 0.1 mM NADH, 4.8 mM F6P, 0.4 mM NaPPI, 0.4 U aldolase, 6 U triosephosphate isomerase, 0.2 U glyceraldehyde-3-phosphate dehydrogenase and 0.025 U fructose-6-phosphate kinase, pyrophosphate-dependent). Absorption changes were followed over 30 min at 30°C. All enzymes were from Sigma.

### Biomass analyses

Biomass was determined by measuring fresh and dry weights. Plant parts were cut into pieces, weighed directly (fresh weight) and weighed again after 3-day incubation at 80°C (dry weight). Thousand-grain weights of seeds were determined with an automated precision counter (model C3, Elmor AG, Schwyz, Switzerland).

### Lipid and protein contents

Crude lipid contents of leaves and seeds were determined according to Wingenter et al. (2010). Leaf disks (1.8 cm diameter) or dried seeds (25 mg) were first homogenized in liquid nitrogen. The crushed material was then resuspended in isopropanol (0.75 ml), transferred to a reaction vial and incubated on a shaker (100 rpm) at 4°C for 12 h. After centrifugation (13 000 g for 10 min), the supernatant was transferred to a pre-weighed reaction vial. After isopropanol evaporation at room temperature, lipid contents were determined by weighing. For total protein contents, leaf disks or seeds (5 mg) were homogenized in 200  $\mu\text{l}$  extraction buffer (50 mM HEPES, 5 mM  $\text{MgCl}_2$ , 15% glycerol, 2% SDS, 1% Triton X-100, 1 mM EDTA and 0.1 mM PMSF) at room temperature. After transfer to a reaction vial and centrifugation at 13000 g for 10 min, the supernatant was diluted 1:5 with bi-distilled water. Protein amounts were determined with the detergent-compatible Pierce™ 660 nm Protein Assay Reagent (ThermoFisher Scientific GmbH, Bremen, Germany).

### Abiotic stress tests

Salt versus drought tolerance during seedling establishment was tested by placing surface-sterilized seeds on MS-agar medium without/with different concentrations of NaCl or mannitol. After stratification for 2 days at 4°C in the dark, plates were transferred to a long day regime (14-h light 21°C/10-h dark 18°C) with germination rates determined after 10 days. Root growth was monitored on vertical plates (Frank et al., 2021). Hard agar medium (MS salts plus vitamins, pH 5.6 with KOH, 1.6% agar) was prepared



without (control) and with different concentrations of NaCl or Mannitol. Surface-sterilized seeds were placed on MS control plates, sealed with Micropore™ tape (3M.com) stratified for 2 days at 4°C and incubated in vertical position under long day regime (16-h light 22°C/8-h dark 20°C) at approximately 140  $\mu\text{mol quanta m}^{-2} \text{sec}^{-1}$  (PAR, at plant height) in a growth chamber (PERCIVAL Model AR-41 L3) using white LEDs at 75% intensity (top level), 64% (centre level) and 75% (bottom level). After 7 days, germinated seedlings were transferred to square petri dishes (12 × 12 cm, Greiner) along a segmented line (colour-coded) to permute all positions of the genotypes (two pairs of seedlings per plate, four plates per condition,  $n = 16$  plants) with three repetitions ( $n = 48$ ). Root tips were marked on Day 7 and scanned on Day 11 (along with a ruler, CanoScan 9000F Mark II; Canon Europe, Amsterdam, The Netherlands). Primary root growth in the 4-day increment was measured using ImageJ (open-source software). For monitoring the response of mature *source* leaves, plants were grown in the greenhouse for 45 days before leaf disks (1.8 cm in diameter) were placed in a microtiter plate with buffer (60 mM Na-phosphate pH 6, 2 mM EDTA, 0.1% Tween-20) and buffer with different concentrations of NaCl or methylviologen for 5 days. To induce salt stress in entire plants, seedlings were grown on MS medium (0.6% agar) under a photoperiod of 14-h light (150  $\mu\text{mol quanta m}^{-2} \text{sec}^{-1}$ ) and 10-h dark at 24°C ( $\pm 1^\circ\text{C}$ ) for 3–4 weeks. A proper volume of salt solution (150 mM NaCl) was spread over the agar, whereas the control received sterile water.

#### Amino acid, proline and NADP(H) measurements

*Source* leaves were harvested at increasing the time after the onset of the light period. For amino acid quantification, plant material was immediately resuspended in 2 ml  $\text{g}^{-1}$  of 3% (w/v) 5-sulphosalicylic acid and extracted with a Teflon-in-glass Potter homogenizer by 20 strokes. The homogenate was centrifuged at RT for 3 min at 12 000  $g$ , before total amino acid and proline contents were measured by the acid ninhydrin method (Forlani & Funck, 2020). NADP(H) levels were quantified by the method of Queval and Noctor (2007). Plant material was harvested, immediately resuspended in 10 ml  $\text{g}^{-1}$  of either 0.2 M HCl or NaOH and quickly extracted as described previously. After centrifugation, supernatant aliquots (240  $\mu\text{l}$ ) were heated at 98°C for 3 min, neutralized by the addition of 24  $\mu\text{l}$  200 mM Na-phosphate buffer (pH 5.6), and a proper volume of 0.2 M NaOH or HCl in a final volume of 480  $\mu\text{l}$  to obtain a pH between 7 and 8. Following further centrifugation, seven sample aliquots (from 6 to 18  $\mu\text{l}$ ) were placed in wells of a microtiter plate in a final volume of 200  $\mu\text{l}$  containing 50 mM HEPES buffer (pH 7.5), 1 mM EDTA, 0.12 mM 2,6-dichlorophenol-indophenol, 1 mM phenazine metasulphate and 0.5 mM glucose-6-phosphate. The reaction was started by adding 0.02  $\mu\text{l}$  of G6PDH suspension (Sigma G7877). The resulting decrease in  $A_{595}$  was monitored at 20-sec intervals for 5 min, and pyridine dinucleotide concentrations were calculated using a calibration curve obtained under the same conditions with known amounts of an authentic NADP(H) standard. Reduced and oxidized forms were distinguished by preferential destruction in acid or base, respectively.

#### Photosynthetic parameters

Chlorophyll-a fluorescence emission was measured in leaves of greenhouse plants with a portable pulse-amplitude-modulated fluorimeter (Junior-PAM; Walz). *Source* leaves were darkened for 1 h and irradiated with actinic light (280  $\mu\text{E}$  intensity) at ambient  $\text{CO}_2$ . Electron transport rates were recorded over 5 min with nine repetitions per genotype.

#### Collection of phloem exudates and leaf disks

Leaves of 6-week-old plants (number 7 from the top) were harvested with a scalpel 2–3 h after illumination in the greenhouse and put in water-filled beakers (two plants per genotype, on 3 consecutive days). In the laboratory, disks were cut from the central leaf part (on both sides of the midrib) and frozen in liquid nitrogen. Flags were prepared from tips by cutting with a razor blade along main veins, leaving a rhomboid area with longer midvein, shortened under water and placed in a reaction vial with 15 mM EDTA pH 7.25 (Tedone et al., 2004). After incubation in a water-saturated translucent box at 150  $\mu\text{E}$  ( $\mu\text{mol quanta m}^{-2} \text{sec}^{-1}$ ) for 5–6 h at 22–23°C in a growth chamber (GroBanks; CLF Plant Climatics), petioles were recut with a razor blade, transferred to another reaction vial (15 mM EDTA pH 7.25) and incubated similarly for 16 h in the dark. Exudate volumes were readjusted with water and heated to 95°C for 3–5 min. Leaf flags were scanned for surface area. Cooled exudates were divided and stored at  $-20^\circ\text{C}$  until analysis/shipping. Sucrose and amino acid contents were measured as described above.

#### Lipid composition analyses

Lipid species were analysed as described in Herrfurth et al. (2021). Leaf disks were freeze-dried and then pulverized with small metal beads by shaking on a vortex. From the phloem exudates, 200  $\mu\text{l}$  were freeze-dried. For lipid analyses by gas chromatography/flame ionization detection (GC/FID), preparation of fatty acid methyl esters (FAMES) was performed as described (Miquel & Browse, 1992) with some modifications. For acidic hydrolysis, 1 ml of a methanolic solution containing 2.75% (v/v)  $\text{H}_2\text{SO}_4$  (95–97%) and 2% (v/v) dimethoxypropane were added to 1 mg leaf tissue or to the freeze-dried phloem exudate. For later fatty acid quantification, 20  $\mu\text{g}$  of triheptadecanoate was added to the leaf tissue or 0.5  $\mu\text{g}$  to the phloem exudate. The sample was incubated for 1 h at 80°C. To extract the resulting FAMES, 1.5 ml of saturated aqueous NaCl solution and 1.2 ml of hexane were added, mixed vigorously and centrifuged at 450  $g$  for 10 min. The hexane phase was dried under streaming nitrogen and redissolved in 0.1 ml acetonitrile. GC analysis was performed with an Agilent 6890 gas chromatograph fitted with a capillary DB-23 column (30 m × 0.25 mm; 0.25  $\mu\text{m}$  coating thickness; J&W Scientific, Agilent, Waldbronn, Germany). Helium was used as carrier gas at a flow rate of 1 ml  $\text{min}^{-1}$ . The temperature gradient was 150°C for 1 min, 150–200°C at 8 K  $\text{min}^{-1}$ , 200–250°C at 25 K  $\text{min}^{-1}$  and 250°C for 6 min. Peak areas were collected with the ChemStation software (Agilent, Waldbronn, Germany).

#### Statistics

Testing for significant differences between the genotypes, ANOVA was employed followed by Tukey's post hoc test in case the data were normally distributed and showed equal variance (Levene's test). Non-parametric statistics were used in case the data were not normally distributed (Wilcoxon signed-rank test followed by the Benjamini–Hochberg procedure to correct for multiple comparisons).

#### ACCESSION NUMBERS

*G6PD3* (At1g24280) was used for heterologous expression in the cytosol (Scharte et al., 2009).

#### ACKNOWLEDGEMENTS

AvS thank Hannes Lansing for assistance with early parallel *Phytophthora* leaf infiltrations and Manuel Frank (Aarhus University,

Denmark) for help with statistical analyses. The authors are grateful for the excellent technical assistance by Ina Schmitz-Thom (CLSM imaging) and Kerstin Fischer (thousand-grain weight determinations) in Münster, as well as Dorothea Meldau and Sabine Freitag (phytohormone measurements) in Göttingen. Further support in Münster was provided by Karin Topp, Wiltrud Krüger, Anna-Maria Azevedo (routine laboratory work) and Dirk Schmidt (care of greenhouse plants). This work was in part supported by a grant from the Deutsche Forschungsgemeinschaft (DFG SCHA 541/12) to AvS. and by the University of Ferrara (FAR 2016) to G.F. Open Access funding enabled and organized by Projekt DEAL.

## FUNDING INFORMATION

This work was financially supported by grants from the Deutsche Forschungsgemeinschaft to A.v.S. (DFG SCHA 541/12). Partial support from the University of Ferrara to G.F. (FAR 2016) is also gratefully acknowledged.

## AUTHOR CONTRIBUTIONS

JS, EW and AvS designed the project. JS, SH, CH, GF and AvS conducted experiments. All authors analysed data. AvS wrote the article with editorial contributions of JS, GF and IF AvS communicated with all co-authors and serves as author for scientific correspondence.

## CONFLICT OF INTEREST

The authors have no conflict of interest to declare.

## SUPPORTING INFORMATION

Additional Supporting Information may be found in the online version of this article.

**Figure S1.** Influence of the cultivation condition on leaf sugar contents.

**Figure S2.** Hormone profiles of non-infiltrated and water- versus zoospore-infiltrated leaves.

**Figure S3.** Seed yields obtained under normal conditions versus drought stress.

**Figure S4.** Abiotic stress tolerance of root and leaf tissue.

**Figure S5.** Tobacco P5CR preferentially uses NADPH in the presence of salt or proline.

**Figure S6.** Amino acid contents and NADPH/NADP<sup>+</sup> ratios in leaves under salt stress.

**Figure S7.** Fatty acid content of leaf tissue used for phloem exudate collection (three series).

**Figure S8.** Efflux from *source* leaves of plants grown under normal or colder conditions.

## REFERENCES

- Allahverdiyeva, Y., Battchikova, N., Brosché, M., Fujii, H., Kangasjärvi, S., Mulo, P. *et al.* (2015) Integration of photosynthesis, development and stress as an opportunity for plant biology. *New Phytologist*, **208**, 647–655.
- Alvarez, M.E., Savouré, A. & Szabados, L. (2022) Proline metabolism as regulatory hub. *Trends in Plant Sciences*, **27**(1), 39–55.
- Andriotis, V.M.E. & Smith, A.M. (2019) The plastidial pentose phosphate pathway is essential for postglobular embryo development in Arabidopsis. *Proceedings of the National Academy of Sciences U S A*, **116**, 15297–15306.
- Baier, M., Bittner, A., Prescher, A. & van Buer, J. (2018) Preparing plants for improved cold tolerance by priming. *Plant, Cell and Environment*, **42**, 782–800.

- Barbaglia, A.M., Tamot, B., Greve, V. & Hoffmann-Benning, S. (2016) Phloem Proteomics Reveals New Lipid-Binding Proteins with a Putative Role in Lipid-Mediated Signaling. *Frontiers in Plant Science*, **7**, 563.
- Batsale, M., Bahammou, D., Fouillen, L., Mongrand, S., Joubès, J. & Domer-gue, F. (2021) Biosynthesis and functions of very-long-chain fatty acids in the responses of plants to abiotic and biotic stresses. *Cells*, **10**, 1284.
- Baune, M.C., Lansing, H., Fischer, K., Meyer, T., Charton, L., Linka, N. *et al.* (2020) The Arabidopsis plastidial glucose-6-phosphate transporter GPT1 is dually targeted to peroxisomes via the endoplasmic reticulum. *The Plant Cell*, **32**, 1703–1726.
- Beinecke, F.A., Grundmann, L., Wiedmann, D.R., Schmidt, F.J., Caesar, A.S., Zimmermann, M. *et al.* (2018) The FT/FD-dependent initiation of flowering under long-day conditions in the day-neutral species *Nicotiana tabacum* originates from the facultative short-day ancestor *Nicotiana tomentosiformis*. *The Plant Journal*, **96**, 329–342.
- Bhagat, P.K., Sharma, D., Verma, D., Singh, K. & Sinha, A.K. (2022) Arabidopsis MPK3 and MPK6 regulate D-glucose signaling and interact with G-protein RGS1. *Plant Science*, **325**, 111484.
- Chang, T.-G. & Zhu, X.-G. (2017) Source-sink interaction: a century old concept under the light of modern molecular systems biology. *Journal of Experimental Botany*, **68**(16), 4417–4431.
- Cho, L.H., Pasriga, R., Yoon, J., Jeon, J.S. & An, G. (2018) Roles of sugars in controlling flowering time. *Journal of Plant Biology*, **61**, 121–130. Available from: <https://doi.org/10.1007/s12374-018-0081-z>
- Curtis, M.J. & Hays, J.B. (2007) Tolerance of dividing cells to replication stress in UVB-irradiated Arabidopsis roots: Requirements for DNA translesion polymerases  $\eta$  and  $\zeta$ . *DNA Repair*, **6**, 1341–1358.
- Dal Santo, S., Stampfl, H., Krasensky, J., Kempa, S., Gibon, Y., Petutschni-g, E. *et al.* (2012) Stress-induced GSK3 regulates the redox stress response by phosphorylating glucose-6-phosphate dehydrogenase in Arabidopsis. *The Plant Cell*, **24**, 3380–3392.
- Dietz, K.-J., Mittler, R. & Noctor, G. (2016) Recent Progress in Understanding the Role of Reactive Oxygen Species in Plant Cell Signaling. *Plant Physiology*, **171**(3), 1535–1539.
- Eckardt, N.A. (2017) The Plant Cell reviews plant immunity: receptor-like kinases, ROS-RLK crosstalk, quantitative resistance, and the growth/defense trade-off. *The Plant Cell*, **29**, 601–602.
- Eicks, M., Maurino, V., Knappe, S., Flügge, U.I. & Fischer, K. (2002) The plastidic pentose phosphate translocator represents a link between the cytosolic and the plastidic pentose phosphate pathways in plants. *Plant Physiology*, **128**, 512–522.
- Engqvist, M.K.M. & Maurino, V.G. (2017) Metabolic Engineering of Photo-respiration. *Methods in Molecular Biology*, **1653**, 137–155.
- Essmann, J., Schmitz-Thom, I., Schön, H., Sonnenwald, S., Weis, E. & Scharte, J. (2008) RNA interference-mediated repression of cell wall invertase impairs defence in *source* leaves of tobacco. *Plant Physiology*, **147**, 1288–1299.
- Farrar, J.F. (1993) Sink strength: What is it and how do we measure it? Introduction. *Plant, Cell and Environment*, **16**, 1015–1016.
- Forlani, G., Bertazzini, M., Zarattini, M., Funck, D., Ruskowski, M. & Nocek, B. (2015) Functional properties and structural characterization of rice  $\delta^1$ -pyrroline-5-carboxylate reductase. *Frontiers in Plant Science*, **6**, 565.
- Forlani, G. & Funck, D. (2020) A specific and sensitive enzymatic assay for the quantitation of L-proline. *Frontiers in Plant Science*, **11**, 582026.
- Frank, M., Kaulfürst-Soboll, H., Fischer, K. & von Schaewen, A. (2021) Complex-type N-glycans influence the root hair landscape of Arabidopsis seedlings by altering the auxin output. *Frontiers in Plant Science*, **12**, 635714.
- Furbank, R.T., Quick, P.O. & Sirault, X.R.R. (2015) Improving photosynthesis and yield potential in cereal crops by targeted genetic manipulation. Prospects, progress, and challenges. *Field Crop Research*, **182**, 19–29.
- Gamir, J., Pastor, V., Sánchez-Bel, P., Agut, B., Mateu, D., García-Andrade, J. *et al.* (2018) Starch degradation, abscisic acid and vesicular trafficking are important elements in callose priming by indole-3-carboxylic acid in response to *Plectosphaerella cucumerina* infection. *The Plant Journal*, **96**, 518–531.
- Ghosh, U.K., Islam, M.N., Siddiqui, M.N., Cao, X. & Khan, M.A.R. (2022) Proline, a multifaceted signalling molecule in plant responses to abiotic stress: understanding the physiological mechanisms. *Plant Biology (Stuttgart)*, **24**(2), 227–239.

- Giberti, S., Funck, D. & Forlani, G. (2014)  $\Delta^1$ -pyrroline-5-carboxylate reductase from *Arabidopsis thaliana*: stimulation or inhibition by chloride ions and feed-back regulation by proline depend on whether NADPH or NADH acts as co-substrate. *New Phytologist*, **202**, 911–919.
- Gómez-Gómez, L., Felix, G. & Boller, T. (1999) A single locus determines sensitivity to bacterial flagellin in *Arabidopsis thaliana*. *The Plant Journal*, **18**, 277–284.
- Guelle, B.S., Benning, U.F. & Hoffmann-Benning, S. (2012) Identification of lipids and lipid-binding proteins in phloem exudates from *Arabidopsis thaliana*. *Journal of Experimental Botany*, **63**, 3603–3616.
- Hake, K. & Romeis, T. (2019) Protein kinase-mediated signalling in priming: Immune signal initiation, propagation, and establishment of long-term pathogen resistance in plants. *Plant, Cell and Environment*, **42**, 904–917.
- Hastilestari, B.R., Lorenz, J., Reid, S., Hofmann, J., Pscheidt, D., Sonnewald, U. et al. (2018) Deciphering source and sink responses of potato plants (*Solanum tuberosum* L.) to elevated temperatures. *Plant, Cell and Environment*, **41**, 2600–2616.
- Hauschild, R. & von Schaewen, A. (2003) Differential regulation of glucose-6-phosphate dehydrogenase isoenzyme activities in potato. *Plant Physiology*, **133**, 47–62.
- He, Z., Webster, S. & He, S.Y. (2022) Growth–defense trade-offs in plants. *Current Biology*, **32**(12), R634–R639.
- Herrfurth, C., Liu, Y.T. & Feussner, I. (2021) Targeted analysis of the plant lipidome by UPLC-NanoESI-MS/MS. In: *Plant lipids: Methods and protocols*. New York, NY: Springer US, pp. 135–155.
- Hölscher, C., Lutterbey, M.C., Lansing, H., Meyer, T., Fischer, K. & von Schaewen, A. (2016) Defects in peroxisomal 6-phosphogluconate dehydrogenase isoform PGD2 prevent gametophytic interaction in *Arabidopsis thaliana*. *Plant Physiology*, **171**, 192–205.
- Ingram, J. & Bartels, D. (1996) The molecular basis of dehydration tolerance in plants. *Annual Review of Plant Physiology and Plant Molecular Biology*, **47**, 377–403.
- Ionescu, I.A., Möller, B.L. & Sánchez-Pérez, R. (2017) Chemical control of flowering time. *Journal of Experimental Botany*, **68**, 369–382.
- Ischebeck, T., Krawczyk, H.E., Mullen, R.T., Dyer, J.M. & Chapman, K.D. (2020) Lipid droplets in plants and algae: Distribution, formation, turnover and function. *Seminars in Cell & Developmental Biology*, **108**, 82–93.
- Jansson, C., Vogel, J., Hazen, S., Brutnell, T. & Mockler, T. (2018) Climate-smart crops with enhanced photosynthesis. *Journal of Experimental Botany*, **69**(16), 3801–3809. Available from: <https://doi.org/10.1093/jxb/ery213>
- Jin, K., Chen, G., Yang, Y., Zhang, Z. & Lu, T. (2022) Strategies for manipulating Rubisco and creating photorespiratory bypass to boost C3 photosynthesis: prospects on modern crop improvement. *Plant, Cell & Environment*, **46**(2), 363–378. Available from: <https://doi.org/10.1111/pce.14500>
- Joshi, R., Singla-Pareek, S.L. & Pareek, A. (2018) Engineering abiotic stress response in plants for biomass production. *Journal of Biological Chemistry*, **293**, 5035–5043.
- Kararov, T.L., Chae, E., Herman, J.J. & Bergelson, J. (2017) Mechanisms to mitigate the trade-off between growth and defense. *The Plant Cell*, **29**, 666–680.
- Kessel-Vigeli, S.K., Wiese, J., Schroers, M.G., Wrobel, T.J., Hahn, F. & Linka, N. (2013) An engineered plant peroxisome and its application in biotechnology. *Plant Science*, **210**, 232–240.
- Kishor, P., Hong, Z., Miao, G.H., Hu, C. & Verma, D. (1995) Overexpression of  $\delta^1$ -pyrroline-5-carboxylate synthetase increases proline production and confers osmotolerance in transgenic plants. *Plant Physiology*, **108**, 1387–1394.
- Korte, P., Unzner, A., Damm, T., Berger, S., Kruschke, M. & Mueller, M.J. (2023) High triacylglycerol turnover is required for efficient opening of stomata during heat stress in *Arabidopsis*. *The Plant Journal*, **115**, 81–96. Available from: <https://doi.org/10.1111/tplj.16210>
- Kovács, H., Aleksza, D., Baba, A.I., Hajdu, A., Király, A.M., Zsigmond, L. et al. (2019) Light control of salt-induced proline accumulation is mediated by ELONGATED HYPOCOTYL 5 in *Arabidopsis*. *Frontiers in Plant Science*, **10**, 1584.
- Kruger, N. & von Schaewen, A. (2003) The oxidative pentose-phosphate pathway: structure and organization. *Current Opinion in Plant Biology*, **6**, 236–246.
- Kuczynski, C., McCorkle, S., Keereetaweep, J., Shanklin, J. & Schwender, J. (2022) An expanded role for the transcription factor WRINKLED1 in the biosynthesis of triacylglycerols during seed development. *Frontiers in Plant Science*, **13**, 955589.
- Kudo, M., Kidokoro, S., Yoshida, T., Mizoi, J., Kojima, M., Takebayashi, Y. et al. (2019) A gene-stacking approach to overcome the trade-off between drought stress tolerance and growth in *Arabidopsis*. *The Plant Journal*, **97**, 240–256.
- Leisner, C.P., Potnis, N. & Sanz-Saez, A. (2022) Crosstalk and trade-offs: plant responses to climate change-associated abiotic and biotic stresses. *Plant, Cell & Environment*, **46**, 2946–2963. Available from: <https://doi.org/10.1111/pce.14532>
- Li, N., Xu, C., Li-Beisson, Y. & Philippar, K. (2016) Fatty acid and lipid transport in plant cells. *Trends in Plant Science*, **21**, 145–158.
- Linnenbrügger, L., Doering, L., Lansing, H., Fischer, K., Eirich, J., Finkemeier, I. et al. (2022) Alternative splicing of *Arabidopsis* G6PD5 recruits NADPH-producing OPPP reactions to the endoplasmic reticulum. *Frontiers in Plant Science*, **13**, 909624.
- Lou, Y., Schwender, J. & Shanklin, J. (2014) FAD2 and FAD3 desaturases form heterodimers that facilitate metabolic channeling in vivo. *Journal of Biological Chemistry*, **289**(26), 17996–18007.
- Madey, E., Nowack, L.M. & Thompson, J.E. (2002) Isolation and characterization of lipid in phloem sap of canola. *Planta*, **214**(4), 625–634.
- Maggio, A., Bressan, R.A., Zhao, Y., Park, J. & Yun, D.J. (2018) It's hard to avoid avoidance: Uncoupling the evolutionary connection between plant growth, productivity and stress "tolerance". *International Journal of Molecular Science*, **19**, E3671.
- Matyash, V., Liebisch, G., Kurzchalia, T.V., Shevchenko, A. & Schwudke, D. (2008) Lipid extraction by methyl-tert-butyl ether for high-throughput lipidomics. *Journal of Lipid Research*, **49**(5), 1137–1146.
- McCormick, A.J. & Kruger, N.J. (2015) Lack of fructose 2,6-bisphosphate compromises photosynthesis and growth in *Arabidopsis* in fluctuating environments. *The Plant Journal*, **81**(5), 670–683.
- Mei, C., Michaud, M., Cussac, M., Albricux, C., Gros, V., Maréchal, E. et al. (2015) Levels of polyunsaturated fatty acids correlate with growth rate in plant cell cultures. *Scientific Reports*, **5**, 15207.
- Meyer, T., Hölscher, C., Schwöppe, C. & von Schaewen, A. (2011) Alternative targeting of *Arabidopsis* plastidic glucose-6-phosphate dehydrogenase G6PD1 involves cysteine-dependent interaction with G6PD4 in the cytosol. *The Plant Journal*, **66**, 745–758.
- Miquel, M. & Browse, J. (1992) *Arabidopsis* mutants deficient in polyunsaturated fatty acid synthesis. Biochemical and genetic characterization of a plant oleoyl-phosphatidylcholine desaturase. *Journal of Biological Chemistry*, **267**, 1502–1509.
- Mittler, R. (2017) ROS Are Good. *Trends in Plant Science*, **22**, 11–19.
- Moore, B.D., Cheng, S.H., Sims, D. & Seemann, J.R. (1999) The biochemical and molecular basis for photosynthetic acclimation to elevated atmospheric CO<sub>2</sub>. *Plant, Cell & Environment*, **22**(6), 567–582. Available from: <https://doi.org/10.1046/j.1365-3040.1999.00432.x>
- Murchie, E.H., Reynolds, M., Slafer, G.A., Foulkes, M.J., Acevedo-Siaca, L., McAusland, L. et al. (2023) A 'wiring diagram' for source strength traits impacting wheat yield potential. *Journal of Experimental Botany*, **74**(1), 72–90.
- Nakamura, Y., Andrés, F., Kanehara, K., Liu, Y., Dörmann, P. & Coupland, G. (2014) *Arabidopsis* florigen FT binds to diurnally oscillating phospholipids that accelerate flowering. *Nature Communications*, **5**, 3553.
- Nakamura, Y., Lin, Y.-C., Watanabe, S., Liu, Y., Katsuyama, K., Kanehara, K. et al. (2019) High-resolution crystal structure of *Arabidopsis* FLOWERING LOCUS T illuminates its phospholipid-binding site in flowering. *iScience*, **21**, 577–586.
- Nielsen, T.H., Rung, J.H. & Villadsen, D. (2004) Fructose-2,6-bisphosphate: a traffic signal in plant metabolism. *Trends in Plant Science*, **9**, 556–563.
- Nowicka, B., Ciura, J., Szymańska, R. & Kruk, J. (2018) Improving photosynthesis, plant productivity and abiotic stress tolerance - current trends and future perspectives. *Journal of Plant Physiology*, **231**, 415–433.
- Okamoto, S., Funck, D., Trovato, M. & Forlani, G. (2016) Editorial: Amino acids of the glutamate family: functions beyond primary metabolism. *Frontiers in Plant Science*, **7**, 318.
- Paul, M.J. & Foyer, C.H. (2001) Sink regulation of photosynthesis. *Journal of Experimental Botany*, **52**, 1383–1400.

- Pugin, A., Frachisse, J.M., Tavernier, E., Bligny, R., Gout, E., Douce, R. *et al.* (1997) Early events induced by the elicitor cryptogin in tobacco cells: Involvement of a plasma membrane NADPH oxidase and activation of glycolysis and the pentose phosphate pathway. *The Plant Cell*, **9**, 2077–2091.
- Queval, G. & Noctor, G. (2007) A plate reader method for the measurement of NAD, NADP, glutathione, and ascorbate in tissue extracts: Application to redox profiling during *Arabidopsis* rosette development. *Analytical Biochemistry*, **363**, 58–69.
- Ralston, A.W. & Hoerr, C.W. (1942) The solubilities of the normal saturated fatty acids. *The Journal of Organic Chemistry*, **7**(6), 546–555.
- Rawsthorne, S. (2002) Carbon flux and fatty acid synthesis in plants. *Progress in Lipid Research*, **41**, 182–196.
- Rivero, R.M., Mittler, R., Blumwald, E. & Zandalinas, S.I. (2022) Developing climate-resilient crops: improving plant tolerance to stress combination. *The Plant Journal*, **109**, 373–389.
- Rodrigues, J., Inzé, D., Nelissen, H. & Saibo, N.J.M. (2019) Source-sink regulation in crops under water deficit. *Trends in Plant Science*, **24**, 652–663.
- Ruiz-Vera, U.M., De Souza, A.P., Long, S.P. & Ort, D.R. (2017) The role of sink strength and nitrogen availability in the down-regulation of photosynthetic capacity in field-grown *Nicotiana tabacum* L. at elevated CO<sub>2</sub> concentration. *Frontiers in Plant Science*, **8**, 998.
- Ruszkowski, M.J., Nocek, B., Forlani, G. & Dauter, Z. (2015) The structure of *Medicago truncatula*  $\delta^1$ -pyrroline-5-carboxylate reductase provides new insights into regulation of proline biosynthesis in plants. *Frontiers in Plant Science*, **6**, 869.
- Sabbioni, G., Funck, D. & Forlani, G. (2021) Enzymology and regulation of  $\delta^1$ -pyrroline-5-carboxylate synthetase 2 from rice. *Frontiers in Plant Science*, **12**, 672702.
- Sanchez-Munoz, R. (2023) Efficient cut and paste: Directional oligodeoxynucleotide-based targeted insertion (DOTI) as a precise genome editing method. *The Plant Cell*, **35**(8), 2697–2698. Available from: <https://doi.org/10.1093/plcell/koad1145>
- Scharte, J., Schön, H., Tjaden, Z., Weis, E. & von Schaewen, A. (2009) Isoenzyme replacement of glucose-6-phosphate dehydrogenase in the cytosol improves stress tolerance in plants. *Proceedings of the National Academy of Sciences U S A*, **106**, 8061–8066.
- Scharte, J., Schön, H. & Weis, E. (2005) Photosynthesis and carbohydrate metabolism in tobacco leaves during an incompatible interaction with *Phytophthora nicotianae*. *Plant, Cell and Environment*, **28**, 1421–1435.
- Shanklin, J. & Cahoon, E.B. (1998) Desaturation and related modifications of fatty acids. *Annual Review of Plant Physiology and Plant Molecular Biology*, **49**, 611–641.
- Shim, Y., Seong, G., Choi, Y., Lim, C., Baek, S.-A., Park, Y.J. *et al.* (2023) Suppression of cuticular wax biosynthesis mediated by rice LOV KELCH REPEAT PROTEIN 2 supports a negative role in drought stress tolerance. *Plant, Cell and Environment*, **46**, 1–17.
- Shinde, S., Villamor, J.G., Lin, W., Sharma, S. & Verslues, P.E. (2016) Proline coordination with fatty acid synthesis and redox metabolism of chloroplast and mitochondria. *Plant Physiology*, **172**, 1074–1088.
- South, P.F., Cavanagh, A.P., Liu, H.W. & Ort, D.R. (2019) Synthetic glycolate metabolism pathways stimulate crop growth and productivity in the field. *Science*, **363**(6422), eaat9077.
- Spector, A.A. (1975) Fatty acid binding to plasma albumin. *Journal of Lipid Research*, **16**(3), 165–179.
- Stampfl, H., Fritz, M., Dal Santo, S. & Jonak, C. (2016) The GSK3/Shaggy-like kinase ASK $\alpha$  contributes to pattern-triggered immunity. *Plant Physiology*, **171**, 1366–1377.
- Stitt, M. (1987) Fructose 2,6-bisphosphate and plant carbohydrate metabolism. *Plant Physiology*, **84**, 201–204.
- Stitt, M. (1990) Fructose 2,6-bisphosphate. In: Rey, P.M. & Harborne, J. (Eds.) *Methods in Plant Biochemistry*, Vol. 3. London: Academic Press, pp. 87–92.
- Stitt, M., von Schaewen, A. & Willmitzer, L. (1991) “Sink” regulation of photosynthetic metabolism in transgenic tobacco plants expressing yeast invertase in their cell wall involves a decrease of the Calvin-cycle enzymes and an increase of glycolytic enzymes. *Planta*, **183**, 40–50.
- Szabados, L. & Savouré, A. (2010) Proline: a multifunctional amino acid. *Trends in Plant Science*, **15**, 89–97.
- Takatsuji, H. (2017) Regulating tradeoffs to improve rice production. *Frontiers in Plant Science*, **8**, 171.
- Tarkowski, Ł.P., Signorelli, S., Considine, M.J. & Montrichard, F. (2022) Integration of reactive oxygen species and nutrient signalling to shape root system architecture. *Plant, Cell and Environment*, **46**(2), 379–390. Available from: <https://doi.org/10.1111/pce.14504>
- Tedone, L., Hancock, R.D., Alberino, S., Haupt, S. & Viola, R. (2004) Long-distance transport of L-ascorbic acid in potato. *BMC Plant Biology*, **4**, 16.
- Ternes, P., Feussner, K., Werner, S., Lerche, J., Iven, T., Heilmann, I. *et al.* (2011) Disruption of the ceramide synthase LOH1 causes spontaneous cell death in *Arabidopsis thaliana*. *New Phytologist*, **192**, 841–854.
- Tugizimana, F., Mhlongo, M.I., Piater, L.A. & Dubery, I.A. (2018) Metabolomics in plant priming research: the way forward? *International Journal of Molecular Sciences*, **19**, 1759.
- Udawat, P., Jha, R.K., Sinha, D., Mishra, A. & Jha, B. (2016) Overexpression of a cytosolic abiotic stress responsive universal stress protein (SbUSP) mitigates salt and osmotic stress in transgenic tobacco plants. *Frontiers in Plant Science*, **7**, 518.
- van Schaftingen, E. & Hers, H.G. (1983) Fructose-2,6-bisphosphate in relation with the resumption of metabolic activity in slices of Jerusalem artichoke tubers. *FEBS Letters*, **164**, 195–200.
- van Schaftingen, E., Lederer, B., Bartrons, R. & Hers, H.G. (1982) A kinetic study of pyrophosphate: fructose-6-phosphate phosphotransferase from potato tubers. Application to a microassay of fructose 2,6-bisphosphate. *European Journal of Biochemistry*, **129**, 191–195.
- Vanhercke, T., El Tahchy, A., Liu, Q., Zhou, X.R., Shrestha, P., Divi, U.K. *et al.* (2014) Metabolic engineering of biomass for high energy density: oilseed-like triacylglycerol yields from plant leaves. *Plant Biotechnology Journal*, **12**, 231–239.
- Villadsen, D. & Nielsen, T.H. (2001) N-terminal truncation affects the kinetics and structure of fructose-6-phosphate 2-kinase/fructose-2,6-bisphosphatase from *Arabidopsis thaliana*. *Biochemical Journal*, **359**, 591–597.
- von Schaewen, A., Langenkämper, G., Graeve, K., Wenderoth, I. & Scheibe, R. (1995) Molecular characterization of the plastidic glucose-6-phosphate dehydrogenase from potato in comparison to its cytosolic counterpart. *Plant Physiology*, **109**, 1327–1335.
- von Schaewen, A., Stitt, M., Schmidt, R., Sonnewald, U. & Willmitzer, L. (1990) Expression of a yeast-derived invertase in the cell wall of tobacco and *Arabidopsis* plants leads to accumulation of carbohydrate and inhibition of photosynthesis and strongly influences growth and phenotype of transgenic tobacco plants. *The EMBO Journal*, **9**, 3033–3044.
- Wakao, S. & Benning, C. (2005) Genome-wide analysis of glucose-6-phosphate dehydrogenases in *Arabidopsis*. *The Plant Journal*, **41**, 243–256.
- Wang, Y., Fan, C., Hu, H., Li, Y., Sun, D., Wang, Y. *et al.* (2016) Genetic modification of plant cell walls to enhance biomass yield and biofuel production in bioenergy crops. *Biotechnology Advances*, **34**, 997–1017.
- Wenderoth, I., Scheibe, R. & von Schaewen, A. (1997) Identification of the cysteine residues involved in redox modification of plant plastidic glucose-6-phosphate dehydrogenase. *Journal of Biological Chemistry*, **272**(43), 26985–26990. Available from: <https://doi.org/10.1074/jbc.272.43.26985>
- Wendt, U.K., Wenderoth, I., Tegeler, A. & von Schaewen, A. (2000) Molecular characterization of a novel glucose-6-phosphate dehydrogenase from potato (*Solanum tuberosum* L.). *The Plant Journal*, **23**, 723–733.
- Wilkinson, J.E., Twell, D. & Lindsey, K. (1997) Activities of CaMV 35S and nos promoters in pollen: implications for field release of transgenic plants. *Journal of Experimental Botany*, **48**, 265–275.
- Wingenter, K., Schulz, A., Wormit, A., Wic, S., Trentmann, O., Hoermiller, I. *et al.* (2010) Increased activity of the vacuolar monosaccharide transporter TMT1 alters cellular sugar partitioning, sugar signaling, and seed yield in *Arabidopsis*. *Plant Physiology*, **154**, 665–677.
- Xue, J., Balamurugan, S., Li, D.-W., Liu, Y.-H., Zeng, H., Wang, L. *et al.* (2017) Glucose-6-phosphate dehydrogenase as a target for highly efficient fatty acid biosynthesis in microalgae by enhancing NADPH supply. *Metabolic Engineering*, **41**, 212–221.
- Yang, L., Wang, X., Chang, N., Nan, W., Wang, S., Ruan, M. *et al.* (2019) Cytosolic Glucose-6-Phosphate Dehydrogenase Is Involved in Seed Germination and Root Growth Under Salinity in *Arabidopsis*. *Frontiers in Plant Science*, **10**, 182.
- Yu, S.M., Lo, S.F. & Ho, T.D. (2015) Source-sink communication: regulated by hormone, nutrient, and stress cross-signaling. *Trends in Plant Science*, **20**, 844–857.

- Yu, X., Feng, B., He, P. & Shan, L. (2017) From chaos to harmony: responses and signaling upon microbial pattern recognition. *Annual Review of Phytopathology*, **55**, 109–137.
- Zhai, Z., Keereetaweep, J., Liu, H., Feil, R., Lunn, J.E. & Shanklin, J. (2018) Trehalose 6-phosphate positively regulates fatty acid synthesis by stabilizing WRINKLED1. *The Plant Cell*, **30**, 2616–2627.
- Zhang, C. & Turgeon, R. (2018) Mechanisms of phloem loading. *Current Opinion in Plant Biology*, **43**, 71–75.
- Zhao, Y., Cui, Y., Huang, S., Yu, J., Wang, X., Xin, D. *et al.* (2020) Genome-wide analysis of the glucose-6-phosphate dehydrogenase family in soybean and functional identification of *GmG6PDH2* involvement in salt stress. *Frontiers in Plant Science*, **11**, 214.